

# The Frequency and Sizes of Inner Bars and Nuclear Rings in Barred Galaxies and Their Dependence on Galaxy Properties

Peter Erwin<sup>1,2</sup>★

<sup>1</sup>Max-Planck-Institute for Extraterrestrial Physics, Giessenbachstr., 85748 Garching, Germany

<sup>2</sup>Universitäts-Sternwarte München, Scheinerstrasse 1, D-81679 München, Germany

Accepted XXX. Received YYY; in original form ZZZ

## ABSTRACT

Using a volume- and mass-limited ( $D < 30$  Mpc,  $\log(M_{\star}/M_{\odot}) \geq 9.75$ ) sample of 155 barred S0–Sd galaxies, I determine the fraction with secondary structures within their bars. Some  $20 \pm 3\%$  have a separate inner bar, making them double-barred; an identical fraction have nuclear rings, with  $11^{+3}_{-2}\%$  hosting both. The inner-bar frequency is a strong, monotonic function of stellar mass: only  $4^{+3}_{-2}\%$  of barred galaxies with  $\log(M_{\star}/M_{\odot}) = 9.75\text{--}10.25$  are double-barred, while  $47 \pm 8\%$  of those with  $\log(M_{\star}/M_{\odot}) > 10.5$  are. The nuclear-ring frequency is a strong function of absolute bar size: only  $1^{+2}_{-1}\%$  of bars with semi-major axes  $< 2$  kpc have nuclear rings, while  $39^{+6}_{-5}\%$  of larger bars do. Both inner bars and nuclear rings are absent in very late-type (Scd–Sd) galaxies.

Inner bar size correlates with galaxy stellar mass, but is clearly offset to smaller sizes from the main population of bars. This makes it possible to define “nuclear bars” in a consistent fashion, based on stellar mass. There are eight single-barred galaxies where the bars are nuclear-bar-sized; some of these may be systems where an outer bar failed to form, or previously double-barred galaxies where the outer bar has dissolved. Inner bar size is even more tightly correlated with host bar size, which is likely the primary driver. In contrast, nuclear ring size is only weakly correlated with galaxy mass or bar size, with more scatter in size than is true of inner bars.

**Key words:** galaxies: structure – galaxies: elliptical and lenticular, cD – galaxies: disc – galaxies: spiral – galaxies: bar

## 1 INTRODUCTION

The interiors of galactic bars can sometimes be rather complex and dramatic places. Instances of double-barred galaxies – where a second, smaller bar is nested inside a large-scale bar, usually with a different orientation – have been known since the 1970s (e.g., de Vaucouleurs 1975; Sandage & Brucato 1979). Examples of nuclear rings – where a ring or pseudoring, often actively star-forming or even starbursting, encircles the nucleus inside the bar – have been known even longer (see references in Buta & Combes 1996).

Double bars first attracted general interest for their possible role in fuelling AGNs. Shlosman et al. (1989) argued that while large-scale bars were known to drive gas to smaller radii, this inflow might stall near the centers of such bars, at radii of a few hundred pc. The presence of a separate inner bar – perhaps formed out of the disc of gas funneled inward by the large-scale bar – could then drive gas inward to smaller scales, where other instabilities might take over. Observational tests of this idea (e.g., Erwin & Sparke 2002; Laine et al. 2002) have generally been inconclusive, however.

More recently, the simulations of Du et al. (2017) suggested that inner bars were more vulnerable to destruction by central supermassive black holes than were large-scale bars, and consequently disrupted

inner bars might be the origin of central (classical) bulges in some galaxies (see also Guo et al. 2020; Nakatsuno & Baba 2023).

There have even been occasional suggestions that the Milky Way itself might be a double-barred galaxy (e.g., Alard 2001; Nishiyama et al. 2005, 2006; Namekata et al. 2009), though the edge-on nature of the Galaxy disk makes it difficult to determine and to distinguish between potentially similar-sized, flattened *axisymmetric* structures such as a nuclear stellar disk (e.g., Gerhard & Martinez-Valpuesta 2012; Valenti et al. 2016).

Nuclear rings have probably been the focus of more research, in part because the presence of significant star formation so close to the center of a galaxy suggests a role in building up the central structure of galaxies in the form of nuclear discs or pseudobulges. The most obvious – and earliest known – examples are naturally those rings with active star formation, though smooth rings of old stars – possibly the faded, fossil remnants of star-forming rings – also exist (e.g., Erwin et al. 2001), as do dusty, gaseous rings without ongoing star formation. As with inner bars, it is possible that the Milky Way hosts a nuclear ring within its bar as well (e.g., Molinari et al. 2011; Henshaw et al. 2016; Sormani et al. 2018).

Currently we have very little idea how common double bars really are; the only surveys to date have either focused on a narrow range of Hubble types (e.g., Erwin & Sparke 2002) or have looked at potentially biased subsets such as Seyfert galaxies (e.g., Laine et al. 2002). The situation for nuclear rings is somewhat better, with

★ E-mail: erwin@mpe.mpg.de

surveys such as [Knapen \(2005\)](#) and the catalog of [Comerón et al. \(2010\)](#). (Some nuclear rings and inner bars are listed in the comprehensive S<sup>4</sup>G analysis of [Herrera-Endoqui et al. 2015](#), but these are limited by the low resolution of the IRAC1 images.) Recent studies of bars have shown that some substructures of bars – in particular, the boxy/peanut-shaped (BP) bulges that are the vertically thickened inner parts of some bars – have very strong dependences on galaxy stellar mass (e.g., [Erwin & Debattista 2017](#); [Li et al. 2017](#); [Kruk et al. 2019](#); [Erwin et al. 2023](#)). So we might wonder if inner bars or nuclear rings might have a similar dependence on stellar mass. This paper is meant to investigate this and related questions by determining the frequency (and sizes) of inner bars and nuclear rings in an unbiased, distance- and mass-limited sample of barred galaxies.

## 2 THE SAMPLE

The foundation of the sample studied here is a survey of S0–Sa barred galaxies presented in [Erwin & Sparke \(2002\)](#) and [Erwin & Sparke \(2003\)](#). This was later extended to include barred Sab and Sb galaxies in [Erwin et al. \(2005\)](#) and [Erwin et al. \(2008\)](#), with additional barred galaxies identified among the corresponding (nominally) unbarred S0–Sb galaxies by [Gutiérrez et al. \(2011\)](#). The original sample was defined to include all northern ( $\delta > -10^\circ$ ) barred galaxies from the Uppsala General Catalog ([Nilson 1973](#)) with heliocentric redshifts  $\leq 2000 \text{ km s}^{-1}$  (roughly speaking,  $D < 28 \text{ Mpc}$ ), RC3 major-axis diameters  $D_{25} \geq 2.0'$ , and RC3 axis ratios  $a/b \leq 2.0$ .

In this paper, I extend the sample concept to cover the full range of bars in regular disks (Hubble types S0–Sd). I also redefine it to have rigorous distance and stellar-mass limits, and drop the original angular-diameter limit. The starting sample is now that defined in the *Spitzer* Survey of Stellar Structure in Galaxies (S<sup>4</sup>G; [Sheth et al. 2010](#)) along with the corresponding Early-Type Galaxies Extension ([Watkins et al. 2022](#)), which corrects for the absence of most elliptical and S0 galaxies in the original S<sup>4</sup>G. (I refer to the combined sample of [Sheth et al. 2010](#) and [Watkins et al. 2022](#) as S<sup>4</sup>G+ETG.) More specifically, I start with all S0–Sd galaxies in S<sup>4</sup>G+ETG (using their optical Hubble types, which come from HyperLEDA),<sup>1</sup> with  $D < 30 \text{ Mpc}$ , stellar masses  $\log(M_\star/M_\odot) > 9.75$ ,<sup>2</sup> and RC3 axis ratios  $a/b \leq 2.0$  (corresponding to inclinations  $i \lesssim 62^\circ$ ). For consistency with previous analyses, and to take advantage of the greater availability of imaging for northern galaxies, I retain the  $\delta > -10^\circ$  limit.

This yielded an initial sample of 279 galaxies. A total of 27 galaxies were discarded for a variety of reasons (e.g., being too highly inclined, despite their RC3 axis ratios or being strongly distorted by interactions or mergers); these rejections are summarized in Appendix B.

I also updated the galaxy distance estimates. Distances in the S<sup>4</sup>G+ETG databases are mostly taken from NED circa 2015 (e.g., [Muñoz-Mateos et al. 2015](#)). A handful of galaxies in the initial sample have more recent direct measurements (Cepheids, TRGB, SBF); in

<sup>1</sup> I exclude two galaxies (NGC 4116 and NGC 4496A) with RC3 types of Sdm and Sm.

<sup>2</sup> The lower limit is meant to make the most of previous analyses of local barred galaxies (e.g., [Erwin & Sparke 2003](#); [Erwin 2011](#)), which extended to masses slightly below  $\log(M_\star/M_\odot) \sim 10$ , as well as to keep the fraction of galaxies observed with *HST* reasonably high. ( $\sim 50\%$  of sample galaxies with  $\log(M_\star/M_\odot) = 9.75$ – $10$  have *HST* data, while only 28% of galaxies that would meet the sample criteria, but with  $\log(M_\star/M_\odot) = 9.0$ – $9.75$ , do.)

addition, I used group distance measurements from [Kourkchi & Tully \(2017\)](#) for galaxies in groups where at least three group members had independent distance measurements. These newer distances were used only if they differed from the S<sup>4</sup>G+ETG values by more than 10%. This led to ten additional galaxies being discarded for having updated distances  $> 30 \text{ Mpc}$ , and one for having a revised stellar-mass estimate below the sample cutoff (see Appendix B). The parent sample then has a total of 242 galaxies; in the next section I describe how this was reduced to the final sample of barred galaxies.

### 2.1 Constructing the Final Sample: Identification of Barred Galaxies

The vast majority of galaxies in the final (barred) sample have been classified as barred in S<sup>4</sup>G or its extension. However, it is worth carefully analyzing all the individual galaxies in order to exclude unbarred galaxies erroneously classified as barred, and to include barred galaxies erroneously classified as unbarred. This was done by visual inspection of the *Spitzer* IRAC1 (3.6 $\mu\text{m}$ ) images that exist for all the galaxies, as well as any available archival *Hubble Space Telescope* (*HST*) images and ground-based images from the Sloan Digital Sky Survey (SDSS; mostly Data Release 7 [Abazajian et al. 2009](#)) and the Siena Galaxy Atlas (SGA; [Moustakas et al. 2023](#)).

The application of this analysis to many of the S0–Sb galaxies in the parent sample has been previously discussed in [Erwin & Sparke \(2003\)](#), [Erwin et al. \(2005\)](#) and [Gutiérrez et al. \(2011\)](#); the latter noted the existence of bars in twelve nominally “unbarred” galaxies (their Table 7).

The following galaxies classified as unbarred in S<sup>4</sup>G+ETG (either in [Buta et al. 2015](#) and [Herrera-Endoqui et al. 2015](#) for S<sup>4</sup>G galaxies or via the “bar family” classification in [Watkins et al. 2022](#)) proved to have bars: NGC 514, NGC 1068 (see [Erwin 2004](#)), NGC 2776, NGC 2964, NGC 3031 ([Gutiérrez et al. 2011](#)), NGC 3599 ([Gutiérrez et al. 2011](#)), NGC 3658, NGC 3982, NGC 3998 ([Gutiérrez et al. 2011](#)), NGC 4041, NGC 4203 ([Erwin & Sparke 2003](#)), NGC 4377, NGC 4736 (see [Erwin 2004](#)), NGC 4750, NGC 4941, NGC 5194/M51a (e.g., [Menéndez-Delmestre et al. 2007](#)), and NGC 5300. Conversely, I found no convincing evidence for bars in NGC 3430, NGC 3949, NGC 4351, NGC 5665, NGC 5958, or NGC 5963.

The final result is a sample of 155 barred galaxies, with 40 S0s and 115 spirals. (The unbarred galaxies amount to 86: 16 S0s and 70 spirals.) These galaxies, along with basic parameters and measurements of the (outer or sole) bars, are listed in Table 1.

### 2.2 Measurements of Disks and Bars

In order to study the sizes of bars and rings, it is usually necessary to correct for projection effects, which will shorten any structures whose major axes are not parallel to the major axis of the disc. This requires knowing the orientation of the disc: its inclination and the position angle of its major axis. These are listed for all galaxies in Table 1. In the vast majority of cases, the disc orientations come from fitting ellipses to the isophotes of the galaxy well outside the bar, using the IRAF task `ellipse`, which implements the algorithm of [Jedrzejewski \(1987\)](#), and assuming that the outer disc (i.e., well outside any bar) is intrinsically circular with a vertical-to-radial axis ratio of  $c/a = 0.2$ . The sources (generally either SDSS, SGA, or IRAC1 images) are listed for individual galaxies in the table. Exceptions – generally cases where, e.g., literature measurements based on gas velocity fields provided more reliable estimates than outer isophotes with

**Table 1.** Barred Galaxy Sample

Name	Type	T	D	$\log M_\star$	Disc PA	$i$	Source	rot	Bar PA	$a_\epsilon$	$L_{\text{bar}}$	$\epsilon_{\text{max}}$	DB?	NR?	FWHM
(1)	(2)	(3)	(Mpc)	( $M_\odot$ )	(deg)	(deg)	(8)	(9)	(deg)	( $''$ )	( $''$ )	(13)	(14)	(15)	( $''$ )
IC 676	(R)SB(r)0 <sup>+</sup>	-1.2	20.0	9.832	15	47	4	-?	164	13	18	0.72			0.15
IC 1067	SB(s)b	3.0	21.9	9.913	120	44	4	-	151	19	19	0.64			0.74
NGC 514	SAB(rs)c	5.2	29.4	10.390	104	48	4	+	154	10	12	0.32			0.15
NGC 600	(R')SB(rs)cd	7.0	22.9	9.793	20	36	3	+	18	15	16	0.68			0.07
NGC 718	SAB(s)a	1.0	21.4	10.283	5	30	4	+	152	20	30	0.44	Y	Y	1.00
NGC 864	SAB(rs)c	5.1	18.8	10.184	23	43	4	+	96	18	23	0.50		Y	0.10

Barred galaxy sample. (1) Galaxy name. (2) Hubble type (Leda). (3) Numerical Hubble type. (4) Distance (from S<sup>4</sup>G+ETG, except as noted). (5) Stellar mass (from S<sup>4</sup>G+ETG, updated for changed distances). (6) Position angle of disc line of nodes. (7) Inclination of disc. (8) Source for disc orientation (1 = SDSS images; 2 = SGA images; 3 = IRAC1 image; 4 = see notes in Appendix C). (9) Sense of galaxy rotation (+ = counter-clockwise, - = clockwise) from spiral arms, if available. (10) Position angle of bar (outer bar in double-barred galaxies). (11) Bar size  $a_\epsilon$ . (12) Bar size  $L_{\text{bar}}$ . (13) Bar maximum ellipticity  $\epsilon_{\text{max}}$ . (14) Galaxy is double-barred. (15) Galaxy has nuclear ring. (16) Full-width-half-maximum of PSF of best available image used to determine DB/NR presence/absence. Notes on alternate distance sources: (a) Cepheids from Saha et al. (2006); (b) SBF from Tonry et al. (2001), with correction from Mei et al. (2005); (c) Group distance from Kourkchi & Tully (2017); (d) Cepheids from Yuan et al. (2020); (e) Virgo Cluster distance from Mei et al. (2007); (f) SBF from Cantiello et al. (2018); (g) Cepheids from Riess et al. (2016). The full table is available in the online version of this paper; I show a representative sample here.

low S/N or distortions due to strong spiral arms – are discussed in Appendix C.

Ellipse fitting is also used to measure the sizes, shapes, and orientations of bars, along with visual inspection to ensure that peaks in the ellipticity profile correspond to a bar rather than to dust extinction, spiral arms, or rings. Erwin (2004) and especially Erwin et al. (2005) provide detailed discussions and examples of this. For consistency with previously published measurements – including the bar measurements for 62 galaxies (17 of them with double bars) (Erwin & Sparke 2003; Erwin 2004; Erwin et al. 2008; Gutiérrez et al. 2011) in this sample – I use  $a_\epsilon$  and  $L_{\text{bar}}$ . The smaller measure,  $a_\epsilon$ , is the semi-major axis of maximum ellipticity in the bar region; sometimes this can be an extremum in the position angle instead, as can be the case when a bar is oriented near the minor axis of a highly inclined galaxy and produces a *minimum* in the ellipticity (see, for example, the cases of NGC 2787, NGC 2880, NGC 3412, NGC 3489, and NGC 4143 in Erwin & Sparke 2003). Following Erwin et al. (2005), the larger size,  $L_{\text{bar}}$ , is intended to be an upper-limit measurement, and is usually the minimum of three measurements: the semi-major axis of the first ellipticity *minimum* outside the bar; the semi-major axis where the isophote PA differs by  $> 10^\circ$  from the bar PA; and the semi-major axis of any spiral arms or rings that visibly cross the end of the bar. Finally, the PA of the bar is taken from a combination of the ellipse fits, visual inspection, and unsharp masking (see the discussion in Erwin & Sparke 2003). The resulting measurements are included in Table 1.

### 3 IDENTIFICATION OF INNER BARS AND NUCLEAR RINGS

The process of identifying inner bars and nuclear rings relies on a combination of visual inspection, fitting ellipses to isophotes, and unsharp masking, applied to optical and near-IR images. Image sources included *Spitzer* IRAC1 images from S<sup>4</sup>G+ETG; optical images from SGA and SDSS; and archival images from *HST*.

**A note on terminology and definitions:** For galaxies with two bars (“double-barred” galaxies), the large bar is the “outer bar” (also known as the “primary bar” in the literature) and the small bar is the

“inner bar” (a.k.a. “secondary bar”). (The question of whether some bars can be called “nuclear bars” will be taken up in Section 6.2.) In galaxies with only one bar, the bar is “single” or “sole”. “Nuclear rings” are defined to be rings (or spiral pseudorings) located *inside* a bar (or inside the outer bar in double-barred systems).

Inner bars are found and measured using the methodology outlined in the preceding section. Unsharp masking is especially important for confirming the presence of weak inner bars and for avoiding confusion due to nuclear spirals, nuclear disks, and nuclear rings, which can on occasion produce similar ellipse-fit signatures (see the examples in Erwin 2004). Figure 1 shows how inner bars can be identified via visual inspection and unsharp masking (NGC 3992 and NGC 4340). The example of NGC 4340 (bottom panels of the figure) highlights the utility of unsharp masks, which in this case show both an inner bar *and* a stellar nuclear ring surrounding the inner bar.

The identification of nuclear rings was made using a combination of visual inspection of images (especially optical images, where both star formation and dust extinction are more prominent than they are in near-IR images – see the example of NGC 3351 in the middle panels of Figure 1) and unsharp masks; the latter are especially useful for identifying stellar nuclear rings (see below).

I sub-classify the nuclear rings a similar fashion to Erwin & Sparke (2003), into star-forming, purely stellar, and purely dusty. The first category includes both actively star-forming rings and rings that are distinctly bluer than the surrounding bar (suggestive of relatively recent star formation). These are usually easy to identify due to their blue colours, patchy nature (the combination of recent sites of localized star formation and dust extinction), and H $\alpha$  emission; see, e.g., Comerón et al. (2010) for numerous examples.<sup>3</sup>

The stellar nuclear rings are smooth circular or oval structures, with colours similar to the surrounding bar, suggesting that they are the fossil remnants of past star-forming rings. These are often best revealed in unsharp masks (Figure 1; see also Erwin & Sparke 1999; Erwin et al. 2001).

<sup>3</sup> Note, however, that Comerón et al.’s “star-forming” nuclear ring class includes the passive, post-star-forming features I call stellar nuclear rings.



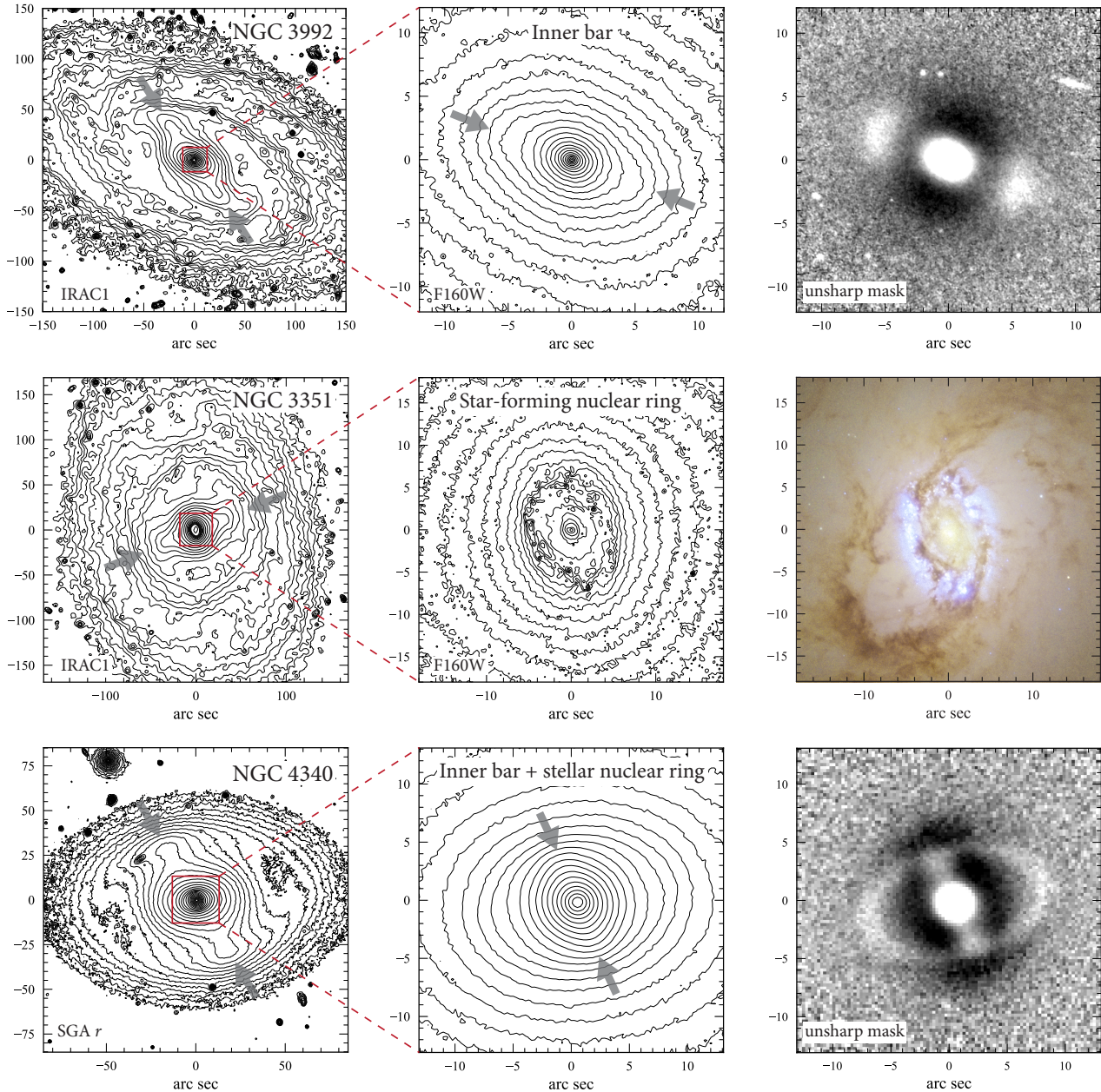


**Figure 1.** Examples of barred galaxies with inner bars and nuclear rings. Contour plots are logarithmically spaced surface brightness; N is up and E is to the left in all panels; large grey arrows indicate bars. **Top row:** SBbc galaxy NGC 3992 (M109), with an inner bar. Left panel =  $S^4G$  IRAC1 image; middle panel = *HST* WFC3-IR F160W image (Proposal ID 15323, PI Walsh); right panel = unsharp mask of F160W image. **Middle row:** SBb galaxy NGC 3351 (M95), with a star-forming nuclear ring; left panel =  $S^4G$  IRAC1 image; middle panel = *HST* WFC3-IR F160W image (Proposal ID 15133, PI Erwin); right panel = WFC3-UVIS UV and optical composite image (F275W, F336W, F438W, F555W, F814W; cropped from original image of ESA/Hubble & NASA). **Bottom row:** SB0 galaxy NGC 4340, with both an inner bar and a (stellar, non-star-forming) nuclear ring. Left and middle panels: SGA  $r$  image; right panel: unsharp mask of same.

Dusty nuclear rings are cases where dust lanes form ringlike or pseudoring structures, *without* evidence for accompanying star formation (or a passive stellar nuclear ring, though these might be obscured by the dust lanes). The assumption is that the rings are more properly *gaseous* rings, made visible in the optical and near-IR by the accompanying dust. These are relatively rare; I find only three clear examples (NGC 2859, NGC 3489, and NGC 5377).

#### 4 FREQUENCIES OF INNER BARS AND NUCLEAR RINGS

There are a total of 31 inner bars in the sample of 155 barred galaxies, so  $20 \pm 3\%$  of the barred galaxies – or  $13 \pm 2\%$  of all the galaxies, barred and unbarred – are double-barred. Their parameters are listed in Table 2. There are also a total of 31 nuclear rings in the sample, with parameters listed in Table 3; the nuclear-ring fraction is thus identical to the double-bar fraction. (Which galaxies are double-barred or nuclear-ring hosts is also indicated in Table 1.) Seventeen

**Table 2.** Inner-bar Measurements for Double-Barred Galaxies

Name	Bar PA (deg)	$a_\epsilon$ (")	$L_{\text{bar}}$ (")	$\epsilon_{\text{max}}$
(1)	(2)	(3)	(4)	(5)
NGC 718	15	1.6	2.2	0.19
NGC 1068	47	15	17	0.45
NGC 2681	20	1.7	3.3	0.26
NGC 2859	62	4.1	6.2	0.31
NGC 2950	85	3.2	3.9	0.33
NGC 3031	140	17	27	0.39

Measurements of inner bars for double-barred galaxies. (1) Galaxy name. (2) Position angle of inner bar. (3) Bar size  $a_\epsilon$ . (4) Bar size  $L_{\text{bar}}$ . (5) Bar maximum ellipticity  $\epsilon_{\text{max}}$ . The full table is available in the online version of this paper; I show a representative sample here.

**Table 3.** Nuclear Ring Measurements

Name	NR PA (deg)	NR $a$ (")	$\epsilon$	Class
(1)	(2)	(3)	(4)	(5)
NGC 718	50	3.3	0.15	blue
NGC 864	110	0.8	0.13	star-forming
NGC 936	130	8.5	0.23	stellar
NGC 1068	50	16	0.32	star-forming
NGC 2608	45	1.1	0.27	star-forming
NGC 2859	60	7.0	0.20	dust

Measurements of nuclear rings. (1) Galaxy name. (2) Position angle of nuclear ring. (3) Semi-major axis. (4) Ellipticity. (5) Nuclear-ring class. The full table is available in the online version of this paper; I show a representative sample here.

of the galaxies host *both* an inner bar *and* a nuclear ring ( $11^{+3}_{-2}\%$  of the barred galaxies, or  $7^{+2}_{-1}\%$  of all the disc galaxies).

A potentially more interesting question than the raw numbers or frequencies in the sample is: how do the fractions of bars with inner bars or nuclear rings depend on galaxy properties? In the following sections, I look at how this might depend on galaxy stellar mass – since the presence of both large-scale bars and B/P bulges inside bars depends strongly on stellar mass (e.g., Erwin & Debattista 2017; Li et al. 2017; Erwin 2018; Erwin et al. 2023) – and also on the size of outer bars (or the only bar in the case of single-barred galaxies) and on Hubble type. I first focus on possible trends, and then use logistic regression to quantify the trends and identify which galaxy parameters might be most important for determining whether a galaxy is double-barred or has a nuclear ring. The stellar masses are all taken from S<sup>4</sup>G+ETG (Muñoz-Mateos et al. 2015; Watkins et al. 2022), except for those galaxies where an updated distance is used (Section 2), for which I recomputed the masses appropriately.

#### 4.1 Inner Bars

Figure 2 shows the frequency of inner bars as a function of galaxy stellar mass for barred galaxies (top panel) and for all galaxies, barred and unbarred (bottom panel).<sup>4</sup> What is quite striking is the very clear and strong mass dependence: inner bars are essentially *absent*

<sup>4</sup> Note that overall bar-fraction trend in the bottom panel (red circles) declines less steeply with stellar mass than was true for the spiral-only sample analyzed

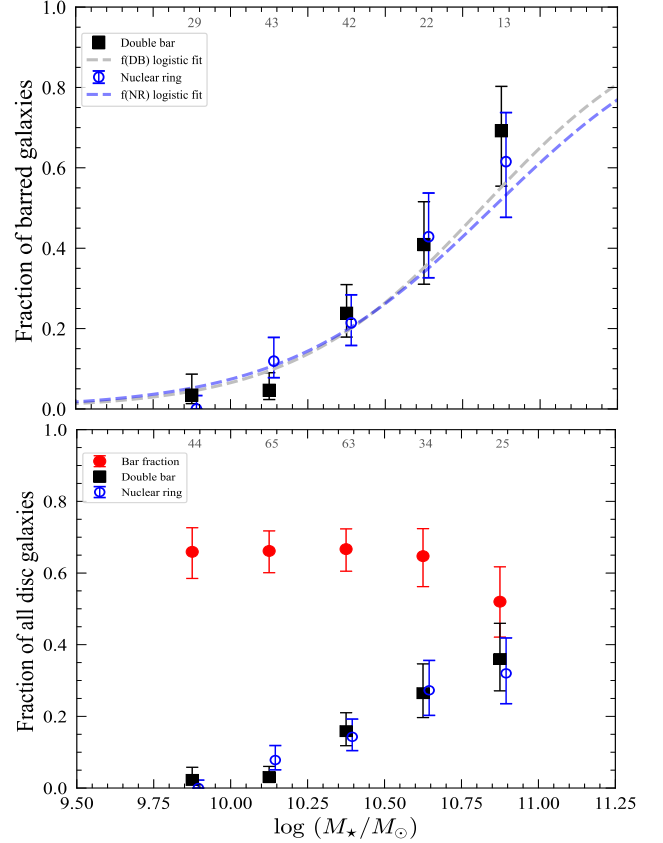


**Figure 2.** Frequency of inner bars (black squares) and nuclear rings (blue circles) in barred S0–Sd galaxies (top) and all S0–Sd galaxies (bottom) as a function of galaxy stellar mass. Dashed curves in the top panel show logistic fits (probability of a galaxy to have the indicated structure) to the underlying data. Red circles in the bottom panel show the fraction of galaxies with at least one bar. The small grey numbers along the tops of each panel give the number of galaxies in each bin. There is a clear trend of both inner bars and nuclear rings becoming more common with increasing stellar mass.

for stellar masses  $\log(M_\star/M_\odot) \lesssim 10$  and then increase steeply in frequency to higher masses, reaching a fraction of  $47 \pm 8\%$  for  $\log(M_\star/M_\odot) > 10.5$  for barred galaxies, or  $26^{+6}_{-5}\%$  when considering all S0–Sd galaxies. The lowest-mass double-barred galaxy is NGC 5770, with  $\log(M_\star/M_\odot) = 9.94$ .

In Figure 4, we can see that inner-bar frequency is *also* a strong function of (outer) bar size: the larger a (large-scale) bar in a galaxy, the higher the chance that it is the outer bar of a double-bar system. No bars with sizes  $< 1$  kpc have inner bars, while almost half ( $48 \pm 9\%$ ) of bars with  $a_\epsilon > 4$  kpc have inner bars.

#### 4.2 Nuclear Rings

Of the 31 nuclear rings in the sample, sixteen are actively forming stars (or, in the case of NGC 718, are blue enough to suggest recent star formation, so I include it in the “star-forming” category), while thirteen are smooth, passive stellar rings. Only three are dusty nuclear rings without evidence for star formation.

Figure 2 shows that the mass trend for nuclear rings as a function of  $\log(M_\star/M_\odot)$  is similar to that for inner bars (see Erwin (2018)). This appears to be due to the inclusion of S0s in this paper’s sample; see Erwin (in prep).

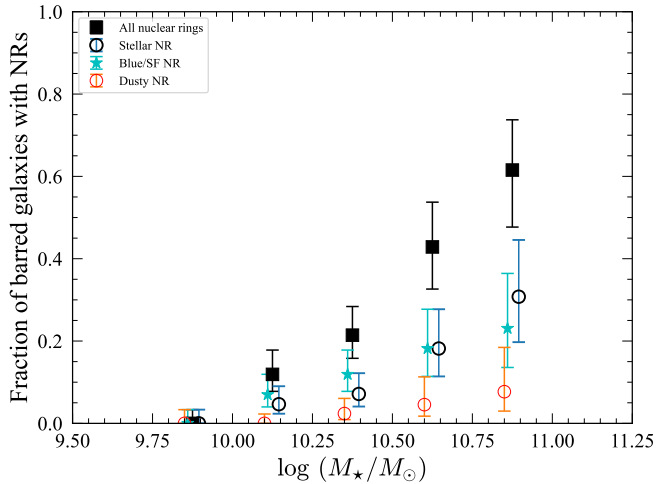


**Figure 3.** Nuclear-ring fraction in barred galaxies for all nuclear rings (black squares) and for different classes of nuclear ring: star-forming (cyan stars), stellar (open black circles), and dust (open orange circles).

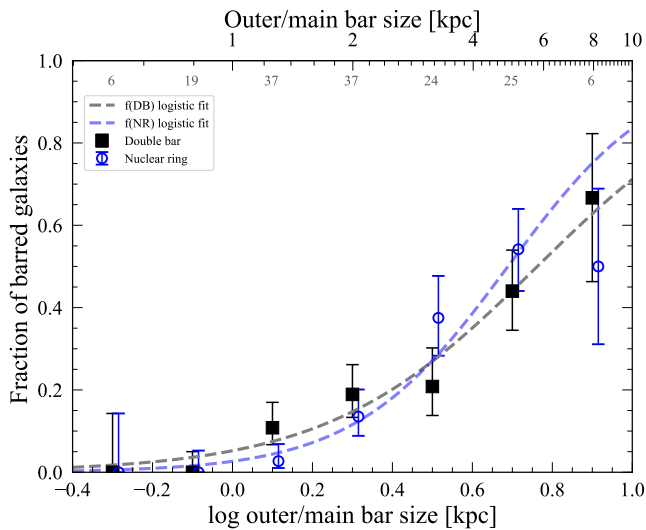


**Figure 4.** Fraction of double bars (black squares) and nuclear rings (open blue circles) for barred galaxies as a function of outer/single bar size ( $a_\epsilon$ ) in kpc. The dashed grey and blue lines are logistic fits for the double-bar (DB) and nuclear-ring (NR) fractions, respectively. Numbers along the top of the plot show the number of galaxies in each (logarithmically spaced) bin.

stellar mass is almost identical to that for inner bars: nuclear rings are absent at low masses, and their frequency increases monotonically to higher masses. The nuclear-ring frequency at the high- and low-mass ends is almost identical to that for inner bars (0% for  $\log(M_*/M_\odot) < 10$ ,  $45 \pm 8\%$  for  $\log(M_*/M_\odot) > 10.5$ ), with nuclear rings being marginally more common at intermediate masses.

The breakdown for the three categories of nuclear ring is shown in Figure 3. Dusty nuclear rings are so rare that no obvious trend is visible. Stellar and star-forming rings show similar trends, increasing in frequency towards higher masses. There is a suggestion that star-forming rings are more abundant in lower-mass galaxies ( $\log(M_*/M_\odot) \sim 10.0\text{--}10.5$ ), while stellar rings are more abundant in the higher-mass galaxies ( $\log(M_*/M_\odot) > 10.5$ ). Given the

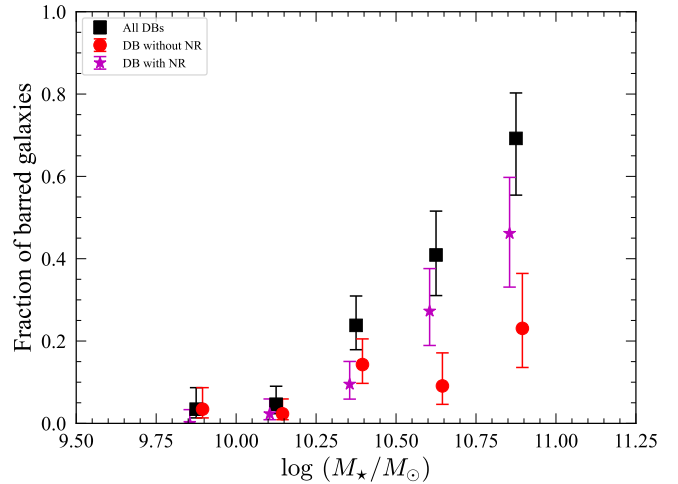


**Figure 5.** Double-bar fraction for all barred galaxies (black squares) and for those barred galaxies also hosting nuclear rings (magenta stars) or those *without* nuclear rings (red circles), as functions of galaxy stellar mass.

uncertainties, however, it is not clear that this difference is really meaningful.

Figure 4 shows that nuclear-ring presence, like inner-bar presence, is a strong function of bar size: only  $1.3^{+2.0}_{-0.8}\%$  of bars with sizes  $< 2$  kpc have nuclear rings, while  $39^{+6}_{-5}\%$  of larger bars do. There is a hint that the nuclear-ring frequency may depend on bar size more strongly than does the inner-bar frequency; inner bars are more common than nuclear rings at smaller bar sizes ( $a_\epsilon \sim 1\text{--}3$  kpc).

### 4.3 Double Bars and Nuclear Rings

The nearly identical frequencies and mass trends for inner bars and nuclear rings suggests a strong association between the two structures – even that they might almost always appear together. Is this the case? Figure 5 investigates this by comparing the stellar-mass trends for all double bars (black squares) as well as for double bars with (magenta stars) and without (red circles) accompanying nuclear rings. In all cases we see a monotonic increase in frequency with stellar mass. The main apparent trend is that in high-mass galaxies, double bars are more likely to coexist with nuclear rings:  $65^{+10}_{-11}\%$  of double bars in galaxies with  $\log(M_*/M_\odot) > 10.5$  are accompanied by nuclear rings, versus only  $38^{+14}_{-12}\%$  in lower-mass galaxies, although the significance of this difference is marginal.

### 4.4 Logistic Regression, Single- and Multi-variable

Since the trends of double-bar and nuclear-ring fraction show such strong and monotonic trends with both stellar mass and bar size, it makes sense to fit for these trends using logistic regression, which uses the logistic equation to describe the probability of an object (such as a barred galaxy) having a binomial characteristic (presence or absence of an inner bar or nuclear ring) as a function of one or more parameters. This process uses all the individual data points directly, and does not depend on any binning scheme (in contrast to the plotted frequency values in the figures).

More precisely, the probability  $P$  of a barred galaxy having a

particular characteristic can be modeled via the logistic equation

$$P = \frac{1}{1 + e^{-(\alpha + \sum_i \beta_i x_i)}}, \quad (1)$$

with  $x_i$  being the different independent variables (e.g., stellar mass or bar size). The probability asymptotes to 0 as  $x_i \rightarrow -\infty$  and to 1 as  $x_i \rightarrow +\infty$  (for  $\beta_i > 0$ , with the reverse behavior for  $\beta_i < 0$ ). If a parameter  $x_i$  has no relation to the probability, then we would expect the corresponding slope  $\beta_i$  to be  $\approx 0$ . I perform the fits using the maximum-likelihood approach of the standard `glm` function in the R statistical language, which provides an estimate of  $P_{\beta=0}$ , the probability for obtaining a slope at least that different from zero under the null hypothesis where the true slope is zero.

The fitting software also provides Akaike Information Criterion (AIC) values for each fit, which can be compared for different models fit to the same data (thus, we can compare AIC values for different models predicting inner-bar frequencies, or for different models predicting nuclear-ring frequencies, but not for both sets of models). Lower values of AIC indicate better fits. One can compute the relative likelihood for two different models (fit to the same dataset) which differ by  $\Delta\text{AIC}$  as  $\exp(\Delta\text{AIC}/2)$ ; in this context, a difference with significance  $P = 0.05$  corresponds to  $\Delta\text{AIC} \approx -6$ , while a  $3\text{-}\sigma$  difference is  $\Delta\text{AIC} \approx -11.5$ .

Table 4 shows the results of the logistic regression analysis for both double bars (upper rows) and nuclear rings. In each case I model the probability as a function of galaxy stellar mass or of absolute bar size (these are the ‘‘Single-Variable Fits’’ in the table).

The very low values of  $P_{\beta=0}$  in all four single-variable fits strongly suggests that the slopes in each fit are different from zero, and that there is a trend (this is not surprising given how strong the trends in binned frequencies appear in Figures 2 and 4). For the case of the double-bar fits, the nearly identical AIC values (differing by  $< 1$ ) indicate that both bar size and stellar mass are equally good predictors of whether a galaxy has a double bar or not. But in the case of nuclear rings, the AIC for the fit using bar size is  $-17.8$  lower than for the fit using stellar mass; this amounts to a  $\sim 3.8\sigma$  significance. So for nuclear rings, bar size is pretty clearly a better predictor than stellar mass.

The top panel of Figure 2 plots the best-fit logistic curves for double-bar and nuclear-ring presence as a function of stellar mass. Although the fits are done to all the individual-galaxy data points and not to the (plotted) binned values, the curves do a reasonably good job of matching the binned frequencies, except possibly at the low-mass end, where the curves may overpredict the frequency of both double bars and nuclear rings. Figure 4 shows the curves when the independent variable is bar size; again, the curves do a good job of matching the binned frequencies.

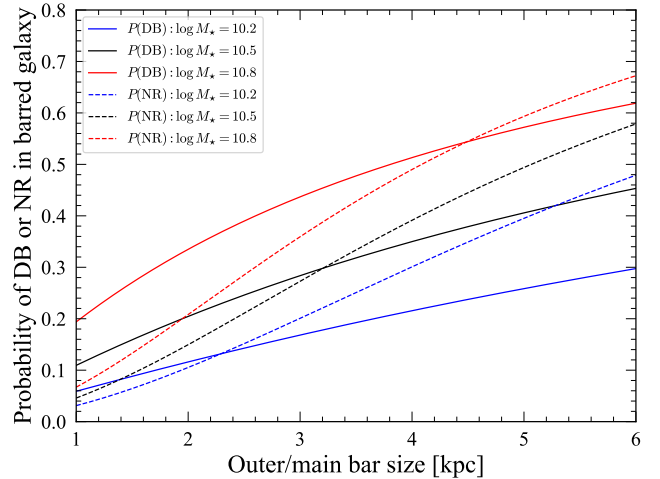
Since bar size and stellar mass are correlated (e.g., Erwin 2019), there is the possibility that the apparent dependence on bar size is a side effect of a more fundamental dependence on stellar mass – or vice versa. (The significantly lower AIC value for the bar-size fit versus the stellar-mass fit for nuclear-ring presence might be an indication of the latter.) To test this, I also fit for double-bar or nuclear-ring presence as a function of *both* stellar mass and bar size simultaneously; these are the ‘‘Multiple-Variable Fits’’ in Table 4. For double bars, the fit using both variables is better than the best single-variable fit ( $\Delta\text{AIC} \approx -6.2$ ), with both variables about equally significant. For nuclear rings, the multi-variable fit is only marginally better than the single-variable fit using bar size, and the  $\log(M_\star/M_\odot)$  slope is not significantly different from zero.

Figure 6 illustrates the combined dependence on stellar mass and bar size for both double bars and nuclear rings as determined by the

**Table 4.** Logistic Regression for DB and NR Presence

Variable	$\alpha$	$\beta$	$P_{\beta=0}$	AIC
(1)	(2)	(3)	(4)	(5)
Presence of Double Bar: Single-Variable Fits				
$\log M_\star$	-35.48	3.28	$6.2 \times 10^{-6}$	133.13
$\log a_\epsilon$	-2.90	3.80	$9.2 \times 10^{-6}$	133.64
Presence of Double Bar: Multiple-variable Fits				
$\log M_\star$	-25.62	2.24	0.0045	126.94
$\log a_\epsilon$		2.45	0.0077	
Presence of Nuclear Ring: Single-Variable Fits				
$\log M_\star$	-32.39	2.99	$1.9 \times 10^{-5}$	136.79
$\log a_\epsilon$	-3.60	5.23	$3.2 \times 10^{-7}$	118.96
Presence of Nuclear Ring: Multiple-variable Fits				
$\log M_\star$	-17.09	1.34	0.094	118.13
$\log a_\epsilon$		4.31	0.00011	

Results of logistic regressions: probability of a barred galaxy being double-barred (upper half of table) or having a nuclear ring (lower half) as function of (log of) galaxy stellar mass or bar size in kpc. In the first part of each section (‘‘Single-Variable Fits’’), each line represents a separate logistic regression; in the second part (‘‘Multiple-Variable Fits’’), it is a single fit using both variables. (1) Galaxy parameter used in fit ( $M_\star$  = stellar mass;  $a_\epsilon$  = semi-major axis of main/outer bar in kpc). (2) Intercept value for fit. (3) Slope for fit. (4)  $P$ -value for slope. (5) Akaike Information Criterion value for fit; lower values indicate better fits.



**Figure 6.** Characteristics of the multi-variable logistic fits for double-bar probability and nuclear-ring probability. Shown are logistic-fit probabilities for a barred galaxy to have an inner bar (solid lines) or a nuclear ring (dashed lines) as a function of outer or single bar size in kpc, for each of three stellar-mass values. Increasing stellar mass increases the probability of double bars and nuclear rings, as does increasing the bar size. Note the steeper curves for the nuclear-ring probability, reflecting the stronger dependence on bar size.

multi-variable logistic fits. In each case, the dependence on bar size when galaxy mass is held fixed is shown by the curves, with individual curves for fixed values of stellar mass ( $\log(M_\star/M_\odot) = 10.2, 10.5,$  and  $10.8$ ). The dependence of double-bar or nuclear-ring probability on stellar mass is clear: the curves are higher for increasing stellar mass. The dependence on bar size is also clear: each individual curve shows probability increasing with increasing bar size. The



fact that the nuclear-ring-probability curves are *steeper* reflects the stronger effect of bar size. For example, if  $\log(M_\star/M_\odot) = 10.5$ , then increasing the bar size from 2 to 4 kpc increases the probability of an inner bar from 20% to 35%, while the same doubling of bar size increases the probability of a nuclear ring from 15% to 39%. Roughly speaking, doubling the bar size increases the chances of finding an inner bar by  $\sim 75\%$ , and almost *triples* the chances of finding a nuclear ring.

In summary, whether or not a barred galaxy has an inner bar is a strong function of stellar mass and a (slightly) weaker function of bar size. Whether it has a nuclear ring is nominally a function of stellar mass – but more significantly a function of bar size; it is plausible that the dependence of nuclear-ring presence on stellar mass is mostly a side effect of the correlation between bar size and stellar mass.

#### 4.5 Trends with Hubble Type

Figure 7 show the fraction of inner bars and nuclear rings as a function of Hubble type. Inner bars are roughly equally common in (HyperLEDA) Hubble types from  $T = -2$  (S0<sup>0</sup>) through 4 (Sbc); none of the 39 barred Sc–Sd galaxies has an inner bar. Nuclear rings follow a similar pattern, though they are notably less abundant for  $T = -2$  and there is a single nuclear ring in a barred Sc galaxy (NGC 864). It seems clear that, unlike the case for stellar mass or bar size, inner bars and nuclear rings do not correlate very strongly with Hubble type, though their absence in Sc–Sd galaxies might be more than just a stellar-mass effect.

### 5 THE SIZES OF INNER BARS AND NUCLEAR RINGS

Moving on from the question of the mere presence or absence of inner bars and nuclear rings, there are a number of potentially interesting characteristics of these structures one might want to investigate. The most straightforward one is *size*, since this only requires deprojecting the observed semi-major axis, and can be directly compared with the size of the outer/sole bar. If we draw on the general population of (large-scale) bar sizes from S<sup>4</sup>G, then we can investigate questions such as: are there inner bars which are larger than the bars of single-barred galaxies? Are the outer bars of double-barred galaxies – or the host bars of nuclear rings – systematically larger (or smaller) than the general population of single bars? How well do the sizes of inner bars or nuclear rings correlate with host-galaxy characteristics like stellar mass, or outer/sole bar size?

Since I have recorded two size estimates for each bar ( $a_\epsilon$  and  $L_{\text{bar}}$ ), it is not immediately obvious which one is the best candidate for comparison with the much larger set of S<sup>4</sup>G bar sizes. Figure 8 compares the S<sup>4</sup>G  $a_{\text{vis}}$  measurements from Herrera-Endoqui et al. (2015) with the corresponding  $a_\epsilon$  and  $L_{\text{bar}}$  sizes for the 78 bars in common between this study and Herrera-Endoqui et al.<sup>5</sup> The closest match to  $a_{\text{vis}}$  is  $a_\epsilon$ , with a median value of  $a_\epsilon/a_{\text{vis}}$  is 0.96; the median of  $L_{\text{bar}}/a_{\text{vis}}$  is 1.16. The extreme outlier is NGC 5248, where the “bar” as defined by Herrera-Endoqui et al. (2015) is a slightly boxy oval region inside the large-scale bar identified by Jogee et al. (2002).

Figure 9 shows the general trend of large-scale bar sizes from non-sample galaxies in S<sup>4</sup>G – specifically, bars with  $a_{\text{vis}}$  measurements from Herrera-Endoqui et al. (2015) – with small gray dots. Also

<sup>5</sup> For NGC 2681, I use the middle bar size; see Section 6.4 for more on this galaxy.

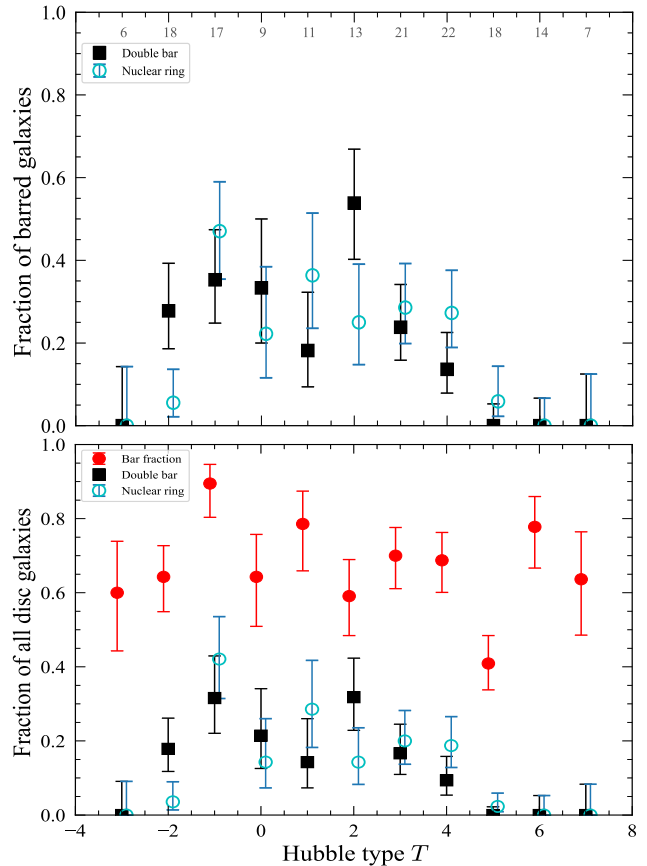


**Figure 7.** As for Figure 2, but now showing frequencies versus Hubble type  $T$ . In contrast to the stellar-mass and bar-size cases (Figures 2 and 4), no clear trends are visible.

shown is the bar-size–stellar-mass broken power-law fit from Erwin (2019), using the thick, dashed blue line. The 1-, 2-, and 3- $\sigma$  bounds of this fit are shown with thinner dashed-blue lines. (These are based on the standard deviation of the residuals of the fit in the region  $\log(M_\star/M_\odot) = 10$ –11; this is  $\sigma = 0.21$  in the  $\log$  of  $a_{\text{vis}}$ .) The large-scale bars from this sample are shown (using  $a_\epsilon$  measurements) with larger filled black circles; these populate the same general trend as the non-sample S<sup>4</sup>G bars, though there is evidence for a population of unusually small bars in this paper’s sample. Those large-scale bars from this study which are *outer* bars of double-barred galaxies are encircled in black. Finally, the *inner* bar sizes from this study are shown with filled red circles.

Several things are apparent from this figure. First, the outer bars of double-barred systems are entirely typical in size for galaxies with their stellar masses; they include both relatively large and relatively small bars. Second, the inner bars are systematically smaller than the general population of bars. This is, of course, no surprise at all, but we can quantify this slightly by noting that inner bar sizes are all below the lower 3- $\sigma$  boundary of the Erwin (2019) power-law fit; they are not simply the low-size tail of the general bar-size distribution. Third, inner-bar size appear to scale with galaxy stellar mass in a manner similar to (identical to?) the way large-scale bars do. The dashed red line is a power-law fit to the inner-bar sizes as a function of stellar mass: the slope is  $0.52^{+0.16}_{-0.14}$ , consistent with the high-mass part of the broken power-law fit to S<sup>4</sup>G bars ( $0.56^{+0.05}_{-0.11}$ , from Table 2 of Erwin 2019).



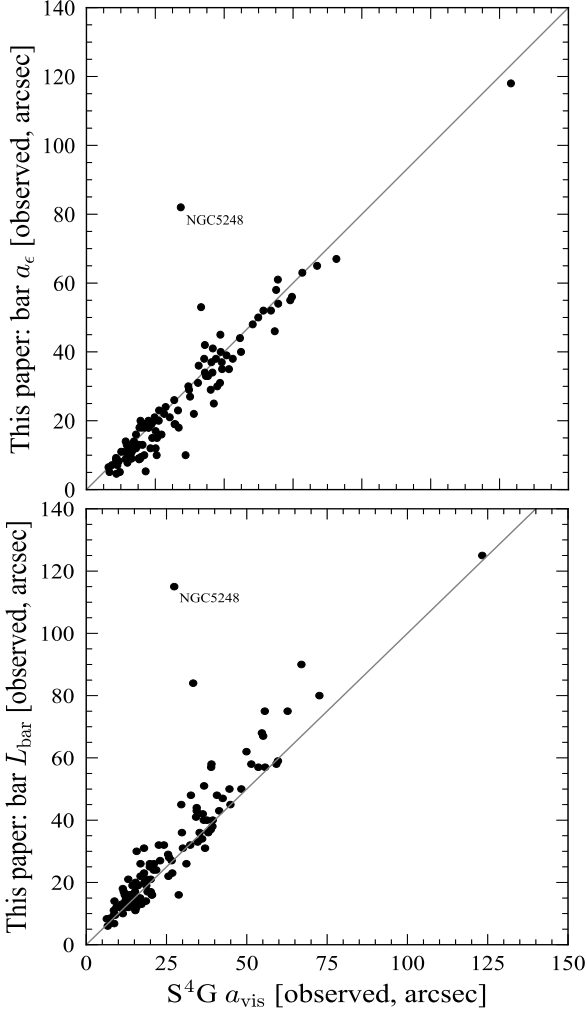


**Figure 8.** Comparison of the two bar-size measurements used in this paper ( $a_\epsilon$  and  $L_{\text{bar}}$ ) with the  $a_{\text{vis}}$  measurement used for S<sup>4</sup>G galaxies by Herrera-Endoqui et al. (2015). The outlier is NGC 5248 (see text).

An obvious question at this point is: given that outer-bar sizes are correlated with galaxy mass (especially for stellar masses  $\log(M_\star/M_\odot) \gtrsim 10.2$ ), could the size-mass correlation of the *inner* bars be a side effect of a primary correlation between the sizes of inner and outer bars? Figure 11 shows that there is indeed a strong correlation between inner and outer bar sizes, with a Spearman correlation coefficient  $r_S = 0.75$  ( $P = 1.2 \times 10^{-6}$ , compared with  $r_S = 0.59$  ( $P = 0.00047$ ) for the correlation with stellar mass. Power-law fits for inner-bar size versus stellar mass and versus outer-bar size are shown in the upper part of Table 5. The bar-size–bar-size fit has a much lower AIC ( $\Delta\text{AIC} \approx -241$ ) and a significantly smaller  $\text{MSE}_{\text{pred}}$  ( $\text{MSE}_{\text{pred}}$  is the mean-squared prediction error, and measures the difference between the actual sizes of inner bars and their predicted sizes according to the fit). Thus, it is clear that inner bar size is primarily correlated with outer bar size, and the correlation with stellar mass is a side effect.

What about nuclear rings? In Figure 10 we can see that nuclear rings can be as small as inner bars, but scatter to larger sizes. Figure 11 shows this is also true when their sizes are plotted against the size of their host bars. A numerical comparison confirms that nuclear rings are, on average, *larger* than inner bars: the median inner-bar size is

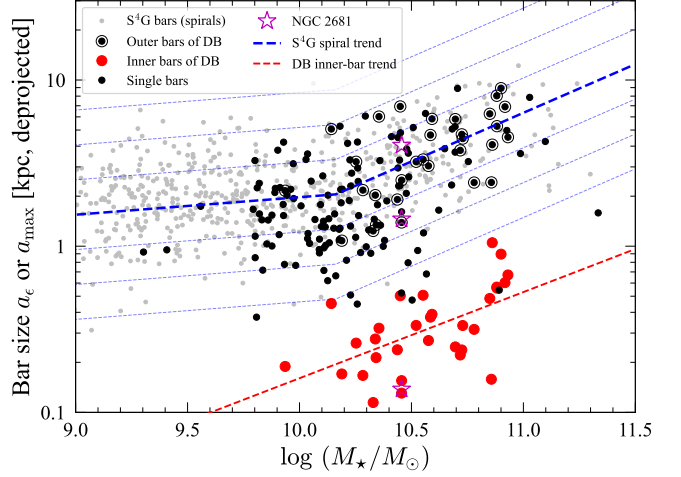


**Figure 9.** Bar size versus galaxy stellar mass. For each galaxy in this sample, the largest (or only) bar is indicated by a filled black circle; if the galaxy is double-barred, then the filled circle is surrounded by a larger open circle. The *inner* bars of double-barred systems are indicated by red circles. Finally,  $a_{\text{vis}}$  measurements from Herrera-Endoqui et al. (2015) for the (large-scale) bars of spiral galaxies in S<sup>4</sup>G from Erwin (2019) that are *not* in this sample are indicated by small grey circles. The dashed red line indicates the power-law fit for inner bars. The thick dashed blue line shows the broken-power-law fit to the bar-size–stellar-mass relation of S<sup>4</sup>G galaxies with  $\log(M_\star/M_\odot) = 9$ –11 from Erwin (2019); the thinner dashed lines show 1-, 2-, and 3- $\sigma$  boundaries, where  $\sigma = 0.21$  is the standard deviation of S<sup>4</sup>G residuals from the fit in the region  $\log(M_\star/M_\odot) = 10$ –11. Finally, the sizes of all three “bars” in the peculiar galaxy NGC 2681 (Section 6.4) are indicated by hollow magenta stars.

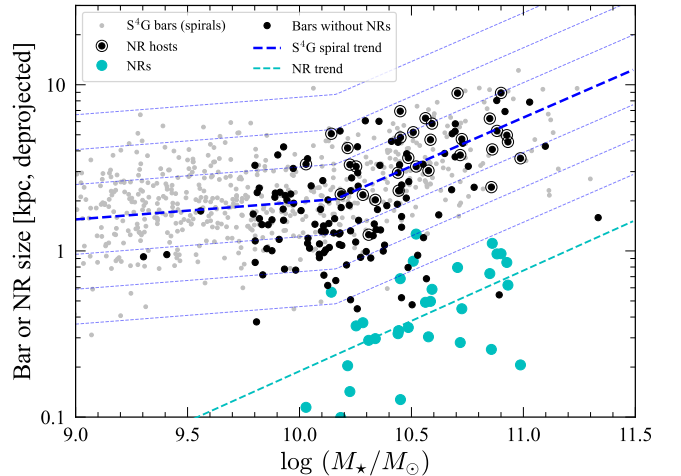


**Figure 10.** As for Figure 9, but showing sizes of nuclear rings (filled cyan circles) and their host bars instead of double-barred systems; the dashed cyan line shows the power-law fit to nuclear-ring sizes.

**Table 5.** Fits for IB/NR Size versus Stellar Mass and Host Bar Size

Predictor (1)	$\alpha$ (2)	$\beta$ (3)	AIC (4)	MSE <sub>pred</sub> (5)
Size of Inner Bar				
$\log M_{\star}$	$-5.98 \pm 1.50$	$0.52 \pm 0.14$	630.1	0.045
$\log a_{\epsilon}$	$-0.90 \pm 0.05$	$0.74 \pm 0.09$	389.2	0.027
Size of Nuclear Ring				
$\log M_{\star}$	$-6.78^{+2.01}_{-1.97}$	$0.61 \pm 0.20$	979.2	0.070
$\log a_{\epsilon}$	$-0.88^{+0.12}_{-0.16}$	$0.82^{+0.22}_{-0.16}$	1000.1	0.068

Results of linear fits for (logarithm of) inner-bar or nuclear-ring size as a function of (logarithm of) galaxy stellar mass and host bar size (outer bar for double-barred galaxies). Parameter uncertainties are based on 2000 rounds of bootstrap resampling. (1) Predictor variable(s). (2) Intercept. (3) Slope. (4) Corrected Akaike Information Criterion value for fit; lower values indicate better fits (comparisons only valid for same dataset). (5) Mean squared prediction error for log of inner-bar or nuclear-ring size (kpc), based on 1000 rounds of bootstrap validation.

315 pc, while the median nuclear-ring size is 370 pc. This is also true if we use sizes relative to the host bar (outer bar for double-barred galaxies): the median inner bar relative size is 0.088 (mean =  $0.10 \pm 0.04$ , range = 0.043–0.26), while the median nuclear-ring size is 0.11 (mean =  $0.12 \pm 0.07$ , range = 0.026–0.39). The results of fitting nuclear-ring size as a function of galaxy mass or bar sizes, in the lower half of Table 5, indicate that stellar mass is formally a better predictor of nuclear-ring size than bar size ( $\Delta\text{AIC} = -20.9$ ), but the MSE<sub>pred</sub> values are basically identical. Although it is tricky to compare fits to different datasets, the MSE<sub>pred</sub> values for the nuclear-ring fits are much larger than the inner-bar fits (0.070 versus 0.027 in the case of fits using (outer) bar size as the predictor), and since the datasets are identical in size, this is probably not a meaningless comparison. It seems clear that inner bars correlate with the sizes of their host bars more strongly than nuclear rings do. (Simulations and theoretical arguments have suggested that nuclear-ring size can depend on a variety of factors, including the rotation curve, bar pattern speeds, and the equation of state of the gas; see, e.g., [Sormani et al. 2023](#) for a discussion and references. Given this, it is perhaps not surprising that nuclear-ring size does not depend strongly on just the size of the bar.)

## 6 DISCUSSION

### 6.1 Comparison with Previous Studies

There have been relatively few studies of the demographics of double-barred galaxies. [Erwin & Sparke \(2002\)](#) studied a distance- and diameter-limited sample of 38 barred S0–Sa galaxies, reporting a frequency of 25% for inner bars. An expanded version of this sample (totalling 76 barred galaxies, including Sab–Sb galaxies) analyzed in [Erwin \(2011\)](#) found a frequency of  $\sim 30\%$ , with no clear trends with Hubble type. The study of [Laine et al. \(2002\)](#) used 56 Seyfert galaxies and 56 matched control galaxies, covering Hubble types S0–Sc. They reported that  $17 \pm 4\%$  of all the galaxies were double-barred (so  $28 \pm 5\%$  of the barred galaxies had inner bars).

These frequencies are higher than I find for the sample in this paper (e.g., a  $20 \pm 3\%$  double-bar fraction for barred galaxies), which can most likely be explained by a bias towards more massive galaxies – which are more likely to have inner bars – in the previous studies, as well as the exclusion of very late-type spirals, which are both

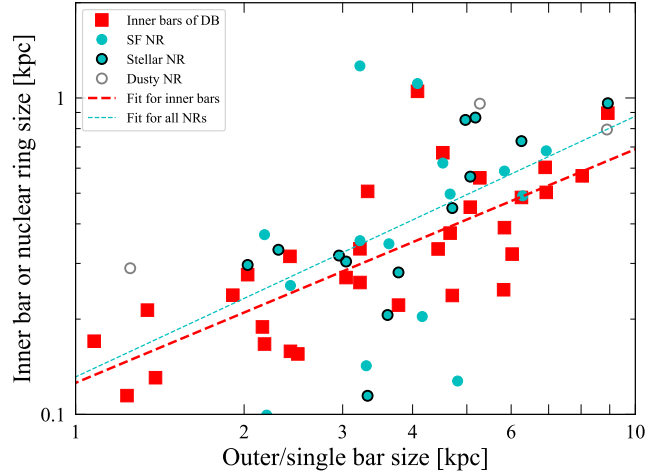


**Figure 11.** Semi-major axes of inner bars (red squares) and nuclear rings (circles) versus host bar semi-major axis. Dashed lines show power-law fits for inner bars (thick red line) and nuclear rings (thin cyan line).

lower mass and lacking inner bars (Section 4.5). For example, the double-bar fraction for barred S0–Sb galaxies in this paper’s sample is  $30 \pm 5\%$ , the same as reported by [Erwin \(2011\)](#) for an earlier (similar but not identical) version of the sample.

Somewhat more attention has been paid to nuclear rings, including the pioneering study of [Buta & Crocker \(1993\)](#) and more recent work by [Knapen \(2005\)](#) and [Comerón et al. \(2010\)](#). [Knapen et al. \(2003\)](#) reported a nuclear-ring fraction of  $21 \pm 5\%$  for their (diameter-limited) sample of 57 spirals. This is about twice the frequency in this paper. As with the double-bar results, this discrepancy can probably be explained by the fact that a diameter-limited sample will be biased towards higher-mass galaxies, which are more likely to host nuclear rings.

[Comerón et al. \(2010\)](#) reported a “star-forming” nuclear-ring fraction of  $20 \pm 2\%$  for Hubble types  $T = -2-7$ . If I exclude the dusty nuclear rings and use the same range of Hubble types, then the fraction of SF+stellar nuclear rings is  $12 \pm 2\%$ . The most plausible reason for the difference is that the Comerón et al. sample is magnitude limited but not distance limited, and so is probably biased in favor of more luminous and thus more massive galaxies – where, as we have seen, the fraction of nuclear rings is higher.

[Herrera-Endoqui et al. \(2015\)](#) looked at nuclear-ring prevalence using S<sup>4</sup>G, which has the advantage of being distance-limited. Unfortunately, the low resolution of the IRAC1 images, the inability to identify dusty nuclear rings due to the minimal dust extinction in the same images, and the absence of unsharp masking as a technique for finding stellar nuclear rings<sup>6</sup> means that most of the nuclear rings found in this paper are missed by the [Buta et al. \(2015\)](#) and [Herrera-Endoqui et al. \(2015\)](#) analysis. Of the 28 S<sup>4</sup>G galaxies with nuclear rings (three more nuclear-ring hosts are S0 galaxies not in S<sup>4</sup>G), only 9 are listed in [Herrera-Endoqui et al. \(2015\)](#).

An important takeaway from all of this is that when the frequencies of particular features (e.g., bars, nuclear rings, etc.) are strongly dependent on some fundamental galaxy parameter (e.g., stellar mass),

<sup>6</sup> Some stellar nuclear rings may show up in [Buta et al. \(2015\)](#) and [Herrera-Endoqui et al. \(2015\)](#) as “nuclear lenses”, but this classification is a mixture of nuclear rings, nuclear discs, and inner bars.

then there is no simple answer to questions like “what fraction of galaxies have features X?”, and answers can be strongly biased by selection effects that depend on the same fundamental parameter (galaxy magnitudes and isophotal diameters are naturally correlated with stellar mass).

## 6.2 Isolated “Nuclear” Bars

Discussions of double-barred galaxies have often involved referring to the inner bars as “nuclear bars”. An extension of this is to suggest that *any* sufficiently small bar is a nuclear bar, even if it is isolated and without an accompanying outer bar. But how are we to define what “sufficiently small” means? It is not unknown to adopt an (arbitrary) semi-major axis of 1 kpc (e.g., Barazza et al. 2009; Melvin et al. 2014). But inspection of the population of (large-scale or outer) bars in local galaxies (e.g., Erwin 2019) shows that the general distribution of bar sizes, even for galaxies with  $\log(M_\star/M_\odot)$  as high as  $\sim 10.1$ , smoothly extends to below 1 kpc. This means it is hard to tell if a strict 1-kpc cutoff is actually a useful way of identifying qualitatively different (single) bars.

Figure 9 suggests a possible solution: we can define a region in the bar-size– $M_\star$  plane which is (mostly) populated by just the *inner* bars in double-barred galaxies, using the existing bar-size– $M_\star$  relation of Erwin (2019), which describes the normal range of outer bars and single bars. Thus, “nuclear bars” are those with semi-major axes smaller than the  $3\text{-}\sigma$  lower limit for the bar-size–stellar-mass relation (the lowest of the dashed thin blue lines in the figure).

The same figure *also* shows that there are eight *single* bars which have sizes characteristic of inner bars. Seven of these – NGC 3982, NGC 3998, NGC 4369, NGC 4041, NGC 4699, NGC 5194 (M51a), and NGC 5713 – are in the same mass range as double-barred galaxies ( $\log(M_\star/M_\odot) \gtrsim 10.1$ ); the eighth (UGC 10803) has  $\log(M_\star/M_\odot) = 9.81$ . All of these bars are sub-kiloparsec in size, ranging in semi-major axis from 370–590 pc – except for NGC 4699 (the most massive galaxy in the sample), which has a bar with  $a_\epsilon = 1.26$  kpc.

Although the classical scenario for double-bar formation involves the inner bar forming *after* the outer bar, usually from gas inflow driven by the outer bar (e.g., Shlosman et al. 1989; Friedli & Martinet 1993; Combes 1994; see also Wozniak 2015), a number of  $N$ -body simulations have inner bars forming first (e.g., Rautiainen & Salo 1999; Debattista & Shen 2007; Du et al. 2015), as does the tidal-interaction scenario identified by Semczuk et al. (2023) from the IllustrisTNG cosmological simulations. In this context, isolated nuclear bars could be cases where a (potential) inner bar formed, but then an outer bar *failed* to form; cases like this were noted in some of the simulations of Du et al. (2015). Alternatively, these could be cases where the galaxy *was* double-barred, but the *outer* bar has dissolved in some fashion, leaving just the inner bar behind. Something like this has also been seen by Du et al. (2015), where some  $N$ -body simulations evolved from double-barred to single-barred when the (weak) outer bars dissolved.

## 6.3 Pattern Speeds: Relative Position Angles Between Inner and Outer Bars

A number of studies have looked at the relative orientation of inner and outer bars in double-barred galaxies. This is because most models of double bars have assumed – or demonstrated in the case of  $N$ -body

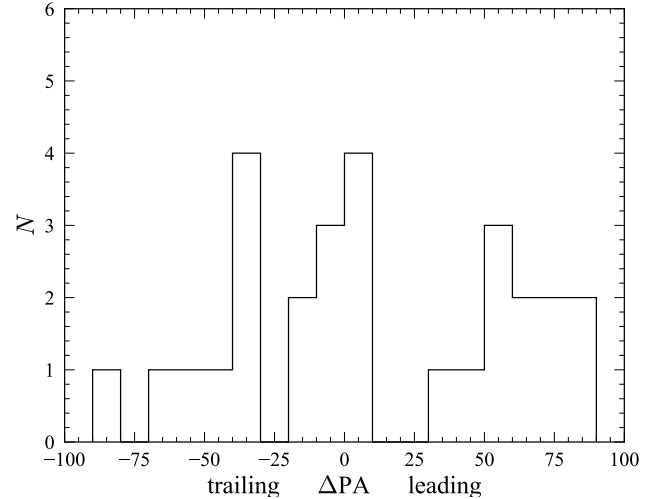


**Figure 12.** Deprojected angles between inner and outer bars of double-barred galaxies. “Leading”/“trailing” refers to whether the inner bar leads or trails the outer bar, assuming the sense of rotation suggested by spiral arms and dust lanes in the galaxy.

models – that the two bars rotate with different pattern speeds,<sup>7</sup> and so should generally have random relative position angles, as has generally been observed (see, e.g., the review in Erwin 2011). In Figure 12 I show the distribution of relative position angles (PA of inner bar – PA of outer bar, deprojected) for the 31 double bars in this sample. There does not appear to be a particular favored relative PA or range of PAs, or a disfavored one; a Kolmogorov-Smirnov test shows no evidence that the distribution is inconsistent with an underlying uniform one ( $P = 0.39$ ). Not surprisingly, then, the distribution is consistent with previous studies and supports the independent-pattern-speed model.

## 6.4 The Peculiar Case of NGC 2681: Triple-Barred Galaxy?

Wozniak et al. (1995) noted the curious case of three galaxies they suggested were, on the basis of ellipse fits to ground-based images, *triple*-barred, with three nested bars. Erwin & Sparke (1999) used *HST* images to show that the apparent ellipse-fit signatures for two of those galaxies (NGC 3945 and NGC 4371) were distorted by the combination of high inclination and large nuclear discs or rings, so that one of the galaxies was merely double-barred and the other had only a single bar. But they also argued that a different, face-on galaxy, NGC 2681, was perhaps genuinely triple-barred. (See also the discussion of this galaxy in Erwin & Sparke 2003.) Laine et al. (2002) claimed to find two triple-barred galaxies, but Erwin (2004) argued that Mrk 573 was only double-barred and NGC 5033 was probably unbarred.

Both NGC 3945 and NGC 4371 are part of this paper’s sample, and remain stubbornly double- and single-barred, respectively.<sup>8</sup> NGC 2681 is also in this sample, and remains a curious, ambiguous case. Figure 9 shows the semi-major axes of all three “bars” in

<sup>7</sup> Note that this does not preclude the pattern speeds being *coupled* in some fashion, such as resonance overlap (e.g., Rautiainen & Salo 1999).

<sup>8</sup> The third of Wozniak et al.’s triple-barred galaxies was NGC 7187, which is not part of this paper’s sample (and which unfortunately still lacks *HST* imaging).

the context of double- and single-barred galaxies. Comparison with other double-barred galaxies strongly suggests the middle and inner bar form a pair that is reasonably typical of double-barred systems (size ratio = 0.094). This makes the outermost bar the peculiar component. (The innermost/outermost size ratio is 0.034, almost half the size of any of the unambiguous double-barred galaxies.)

## 7 SUMMARY

I have presented the results of a search for inner bars and nuclear rings in a volume- and mass-limited sample of 155 barred S0–Sd galaxies, located at distances  $< 30$  Mpc with stellar masses  $\log(M_*/M_\odot) > 9.75$ . An equal fraction ( $20 \pm 3\%$ ) of the galaxies have an inner bar (making them double-barred) and/or a nuclear ring;  $11^{+3}_{-2}\%$  of the galaxies have *both*.

The frequency of both inner bars and nuclear rings is a strong function of stellar mass: more massive galaxies are more likely to have either an inner bar or a nuclear ring (or both). 47% of the barred galaxies with stellar masses  $\log(M_*/M_\odot) > 10.5$  are double-barred, and 45% have nuclear rings; approximately one-third have both an inner bar and a nuclear ring.

However, the *strongest* determinant of nuclear-ring presence is actually the linear size (semi-major axis in kpc) of the host bar. Approximately 40% of bars with semi-major axes  $> 2$  kpc have nuclear rings, while barely  $\sim 1\%$  of smaller bars do. The dependence of nuclear ring presence on stellar mass appears to be simply a side effect of the general correlation between (large-scale) bar size and stellar mass (e.g., [Erwin 2019](#)). For inner bars, (outer) bar size is a strong determinant, but does not dominate over stellar mass as it does for nuclear rings.

The size of inner bars correlates with stellar mass, but correlates more strongly with outer-bar size; inner bars have a median semi-major axis 0.09 times that of their host (outer) bars, with the relative sizes ranging from 0.043 to 0.26. Nuclear rings also scale with host bar size, but the correlation is weaker and the scatter in size is larger (median ring-radius = 0.11 of bar size, ranging from 0.026 to 0.39).

The correlation of both outer/sole bars and inner bars with stellar mass enables one to operationally define “nuclear bars” as a function of stellar mass: bars with sizes more than  $3\text{-}\sigma$  below the general bar-size–stellar-mass relation of [Erwin \(2019\)](#). This makes it possible to identify eight galaxies with nuclear bars but no large-scale bars; these might represent galaxies which formed a potential inner bar but then failed to form an accompanying outer bar, or which were originally double-barred but have had their outer bar weaken and dissolve.

Finally, I note that given that the Milky Way is an Sbc spiral with a stellar mass of  $\log(M_*/M_\odot) \sim 10.5$  ([Bland-Hawthorn & Gerhard 2016](#)) and a bar semi-major axis of  $\sim 4$  kpc ([Wegg et al. 2015](#)),<sup>9</sup> we can use the logistic-regression results of Section 4.4 and the fits of Section 5 to predict a 41% chance of there being an inner bar (with a most probable radial size of  $\sim 350$  pc), and a 39% chance of there being a nuclear ring (with little in the way of size constraints).

<sup>9</sup> Wegg et al. suggest a maximum bar semi-major axis of 5 kpc; since the fits in this paper use the semi-major axis of maximum ellipticity  $a_e$  as the bar size, I adopt  $0.8 \times 5 = 4$  kpc, based on the finding that  $a_e$  is typically  $\sim 0.8$  times the maximum-size estimate of  $L_{\text{bar}}$  in [Erwin \(2005\)](#).

## ACKNOWLEDGMENTS

This work has benefitted from comments by and conversations with Lia Athanassoula, Min Du, Isaac Shlosman, Witold Maciejewski, Kanak Saha, Françoise Combes, John Beckman, Stuart Robert Anderson, Mattia Sormani, and especially Victor Debattista. I also thank Preben Grosbøl for supplying near-IR images of several galaxies, and the anonymous referee for a number of helpful comments.

This research is based on observations made with the NASA/ESA *Hubble Space Telescope*, obtained from the data archive at the Space Telescope Institute. STScI is operated by the association of Universities for Research in Astronomy, Inc. under the NASA contract NAS 5-26555.

This work is based in part on observations made with the *Spitzer* Space Telescope, obtained from the NASA/IPAC Infrared Science Archive, both of which are operated by the Jet Propulsion Laboratory, California Institute of Technology under a contract with the National Aeronautics and Space Administration. This paper also makes use of data obtained from the Isaac Newton Group Archive which is maintained as part of the CASU Astronomical Data Centre at the Institute of Astronomy, Cambridge.

The Legacy Surveys consist of three individual and complementary projects: the Dark Energy Camera Legacy Survey (DECaLS; Proposal ID #2014B-0404; PIs: David Schlegel and Arjun Dey), the Beijing-Arizona Sky Survey (BASS; NOAO Prop. ID #2015A-0801; PIs: Zhou Xu and Xiaohui Fan), and the Mayall z-band Legacy Survey (MzLS; Prop. ID #2016A-0453; PI: Arjun Dey). DECaLS, BASS and MzLS together include data obtained, respectively, at the Blanco telescope, Cerro Tololo Inter-American Observatory, NSF’s NOIRLab; the Bok telescope, Steward Observatory, University of Arizona; and the Mayall telescope, Kitt Peak National Observatory, NOIRLab. The Legacy Surveys project is honoured to be permitted to conduct astronomical research on Iolkam Du’ag (Kitt Peak), a mountain with particular significance to the Tohono O’odham Nation.

NOIRLab is operated by the Association of Universities for Research in Astronomy (AURA) under a cooperative agreement with the National Science Foundation.

This project used data obtained with the Dark Energy Camera (DECam), which was constructed by the Dark Energy Survey (DES) collaboration. Funding for the DES Projects has been provided by the U.S. Department of Energy, the U.S. National Science Foundation, the Ministry of Science and Education of Spain, the Science and Technology Facilities Council of the United Kingdom, the Higher Education Funding Council for England, the National Center for Supercomputing Applications at the University of Illinois at Urbana-Champaign, the Kavli Institute of Cosmological Physics at the University of Chicago, Center for Cosmology and Astro-Particle Physics at the Ohio State University, the Mitchell Institute for Fundamental Physics and Astronomy at Texas A&M University, Financiadora de Estudos e Projetos, Fundação Carlos Chagas Filho de Amparo, Financiadora de Estudos e Projetos, Fundação Carlos Chagas Filho de Amparo à Pesquisa do Estado do Rio de Janeiro, Conselho Nacional de Desenvolvimento Científico e Tecnológico and the Ministério da Ciência, Tecnologia e Inovações, the Deutsche Forschungsgemeinschaft and the Collaborating Institutions in the Dark Energy Survey. The Collaborating Institutions are Argonne National Laboratory, the University of California at Santa Cruz, the University of Cambridge, Centro de Investigaciones Energéticas, Medioambientales y Tecnológicas-Madrid, the University of Chicago, University College London, the DES-Brazil Consortium, the University of Edinburgh, the Eidgenössische Technische Hochschule (ETH) Zürich, Fermi National Accelerator Laboratory, the University of Illinois at



Urbana-Champaign, the Institut de Ciències de l'Espai (IEEC/CSIC), the Institut de Física d'Altes Energies, Lawrence Berkeley National Laboratory, the Ludwig Maximilians Universität München and the associated Excellence Cluster Universe, the University of Michigan, NSF's NOIRLab, the University of Nottingham, the Ohio State University, the University of Pennsylvania, the University of Portsmouth, SLAC National Accelerator Laboratory, Stanford University, the University of Sussex, and Texas A&M University.

BASS is a key project of the Telescope Access Program (TAP), which has been funded by the National Astronomical Observatories of China, the Chinese Academy of Sciences (the Strategic Priority Research Program “The Emergence of Cosmological Structures” Grant # XDB09000000), and the Special Fund for Astronomy from the Ministry of Finance. The BASS is also supported by the External Cooperation Program of Chinese Academy of Sciences (Grant # 114A11KY5B20160057), and Chinese National Natural Science Foundation (Grant # 11433005).

The Legacy Survey team makes use of data products from the Near-Earth Object Wide-field Infrared Survey Explorer (NEOWISE), which is a project of the Jet Propulsion Laboratory/California Institute of Technology. NEOWISE is funded by the National Aeronautics and Space Administration.

The Legacy Surveys imaging of the DESI footprint is supported by the Director, Office of Science, Office of High Energy Physics of the U.S. Department of Energy under Contract No. DE-AC02-05CH1123, by the National Energy Research Scientific Computing Center, a DOE Office of Science User Facility under the same contract; and by the U.S. National Science Foundation, Division of Astronomical Sciences under Contract No. AST-0950945 to NOAO.

The Siena Galaxy Atlas was made possible by funding support from the U.S. Department of Energy, Office of Science, Office of High Energy Physics under Award Number DE-SC0020086 and from the National Science Foundation under grant AST-1616414.

This research also made use of both the NASA/IPAC Extragalactic Database (NED) which is operated by the Jet Propulsion Laboratory, California Institute of Technology, under contract with the National Aeronautics and Space Administration, and the Lyon-Meudon Extragalactic Database (HyperLEDA; <http://leda.univ-lyon1.fr>).

Finally, this research made use of Astropy, a community-developed core Python package for Astronomy ([Astropy Collaboration et al. 2022](https://astropy.org)).

## DATA AVAILABILITY

The data underlying this article, along with code for reproducing fits and figures, are available at [https://github.com/perwin/db-nr\\_paper](https://github.com/perwin/db-nr_paper) and also at <https://doi.org/10.5281/zenodo.10252783>.

## REFERENCES

- Abazajian K. N., et al., 2009, *ApJS*, 182, 543  
 Aguerri J. A. L., Méndez-Abreu J., Corsini E. M., 2009, *A&A*, 495, 491  
 Alard C., 2001, *A&A*, 379, L44  
 Astropy Collaboration et al., 2022, *ApJ*, 935, 167  
 Barazza F. D., et al., 2009, *A&A*, 497, 713  
 Bland-Hawthorn J., Gerhard O., 2016, *ARA&A*, 54, 529  
 Bosma A., Goss W. M., Allen R. J., 1981, *A&A*, 93, 106  
 Buta R., Combes F., 1996, *Fundamentals Cosmic Phys.*, 17, 95  
 Buta R., Crocker D. A., 1993, *AJ*, 105, 1344  
 Buta R. J., et al., 2015, *ApJS*, 217, 32  
 Cantiello M., et al., 2018, *ApJ*, 856, 126  
 Combes F., 1994, in Shlosman I., ed., *Mass-Transfer Induced Activity in Galaxies*. p. 170  
 Comerón S., Knapen J. H., Beckman J. E., Laurikainen E., Salo H., Martínez-Valpuesta I., Buta R. J., 2010, *MNRAS*, 402, 2462  
 Comerón S., et al., 2014, *A&A*, 562, A121  
 Davies R. I., et al., 2014, *ApJ*, 792, 101  
 Debattista V. P., Shen J., 2007, *ApJ*, 654, L127  
 Du M., Shen J., Debattista V. P., 2015, *ApJ*, 804, 139  
 Du M., Debattista V. P., Shen J., Ho L. C., Erwin P., 2017, *ApJ*, 844, L15  
 Elmegreen D. M., Chromey F. R., Johnson C. O., 1995, *AJ*, 110, 2102  
 Epinat B., et al., 2008, *MNRAS*, 388, 500  
 Erwin P., 2004, *A&A*, 415, 941  
 Erwin P., 2005, *MNRAS*, 364, 283  
 Erwin P., 2011, *Mem. S. A. It. Suppl.*, 18, 145  
 Erwin P., 2018, *MNRAS*, 474, 5372  
 Erwin P., 2019, *MNRAS*, 489, 3553  
 Erwin P., Debattista V. P., 2013, *MNRAS*, 431, 3060  
 Erwin P., Debattista V. P., 2017, *MNRAS*, 468, 2058  
 Erwin P., Sparke L. S., 1999, *ApJL*, 521, L37  
 Erwin P., Sparke L. S., 2002, *AJ*, 124, 65  
 Erwin P., Sparke L. S., 2003, *ApJS*, 146, 299  
 Erwin P., Vega Beltrán J. C., Beckman J. E., 2001, in J. H. Knapen, J. E. Beckman, I. Shlosman, & T. J. Mahoney ed., *The Central Kiloparsec of Starbursts and AGN: The La Palma Connection*. p. 171  
 Erwin P., Vega Beltrán J. C., Graham A. W., Beckman J. E., 2003, *ApJ*, 597, 929  
 Erwin P., Beckman J. E., Pohlen M., 2005, *ApJL*, 626, L81  
 Erwin P., Pohlen M., Beckman J. E., 2008, *AJ*, 135, 20  
 Erwin P., et al., 2015, *MNRAS*, 446, 4039  
 Erwin P., et al., 2021, *MNRAS*, 502, 2446  
 Erwin P., Debattista V. P., Anderson S. R., 2023, *MNRAS*, 524, 3166  
 Fathi K., Beckman J. E., Piñol-Ferrer N., Hernandez O., Martínez-Valpuesta I., Carignan C., 2009, *ApJ*, 704, 1657  
 Friedli D., Martinet L., 1993, *A&A*, 277, 27  
 Gerhard O., Martínez-Valpuesta I., 2012, *ApJ*, 744, L8  
 Guo M., Du M., Ho L. C., Debattista V. P., Zhao D., 2020, *ApJ*, 888, 65  
 Gutiérrez L., Erwin P., Aladro R., Beckman J. E., 2011, *AJ*, 142, 145  
 Haan S., Schinnerer E., Mundell C. G., García-Burillo S., Combes F., 2008, *AJ*, 135, 232  
 Henshaw J. D., et al., 2016, *MNRAS*, 457, 2675  
 Hernandez O., Carignan C., Amram P., Chemin L., Daigle O., 2005, *MNRAS*, 360, 1201  
 Herrera-Endoqui M., Díaz-García S., Laurikainen E., Salo H., 2015, *A&A*, 582, A86  
 Hewitt J. N., Haynes M. P., Giovanelli R., 1983, *AJ*, 88, 272  
 Higdon J. L., Buta R. J., Purcell G. B., 1998, *AJ*, 115, 80  
 Jedrzejewski R. I., 1987, *MNRAS*, 226, 747  
 Jensen J. B., et al., 2021, *ApJS*, 255, 21  
 Jogee S., Knapen J. H., Laine S., Shlosman I., Scoville N. Z., Englmaier P., 2002, *ApJ*, 570, L55  
 Knapen J. H., 2005, *A&A*, 429, 141  
 Knapen J. H., de Jong R. S., Stedman S., Bramich D. M., 2003, *MNRAS*, 344, 527  
 Kourkchi E., Tully R. B., 2017, *ApJ*, 843, 16  
 Kruk S. J., Erwin P., Debattista V. P., Lintott C., 2019, *MNRAS*, 490, 4721  
 Laine S., Shlosman I., Knapen J. H., Peletier R. F., 2002, *ApJ*, 567, 97  
 Laurikainen E., Salo H., Buta R., 2005, *MNRAS*, 362, 1319  
 Levy R. C., et al., 2018, *ApJ*, 860, 92  
 Li Z.-Y., Ho L. C., Barth A. J., 2017, *ApJ*, 845, 87  
 Liang X., Yu S.-Y., Fang T., Ho L. C., 2023, *arXiv e-prints*, p. arXiv:2311.04019  
 Liszt H. S., Dickey J. M., 1995, *AJ*, 110, 998  
 Mei S., et al., 2005, *ApJ*, 625, 121  
 Mei S., et al., 2007, *ApJ*, 655, 144  
 Melvin T., et al., 2014, *MNRAS*, 438, 2882  
 Menéndez-Delmestre K., Sheth K., Schinnerer E., Jarrett T. H., Scoville N. Z., 2007, *ApJ*, 657, 790

- Moellenhoff C., Matthias M., Gerhard O. E., 1995, *A&A*, 301, 359
- Molinari S., et al., 2011, *ApJ*, 735, L33
- Moustakas J., et al., 2023, arXiv e-prints, p. arXiv:2307.04888
- Muñoz-Mateos J. C., et al., 2015, *ApJS*, 219, 3
- Nakatsuno N., Baba J., 2023, arXiv e-prints, p. arXiv:2308.15029
- Namekata D., Habe A., Matsui H., Saitoh T. R., 2009, *ApJ*, 691, 1525
- Nilson P., 1973, *Uppsala General Catalogue of Galaxies. Acta Universitatis Upsaliensis. Nova Acta Regiae Societatis Scientiarum Upsaliensis - Uppsala Astronomiska Observatoriums Annaler*, Uppsala: Astronomiska Observatorium, 1973
- Nishiyama S., et al., 2005, *ApJ*, 621, L105
- Nishiyama S., Nagata T., IRSF/SIRIUS Team 2006, in *Journal of Physics Conference Series*. pp 62–66
- Nowak N., Thomas J., Erwin P., Saglia R. P., Bender R., Davies R. I., 2010, *MNRAS*, 403, 646
- Pedlar A., Howley P., Axon D. J., Unger S. W., 1992, *MNRAS*, 259, 369
- Ponomareva A. A., Verheijen M. A. W., Bosma A., 2016, *MNRAS*, 463, 4052
- Rautiainen P., Salo H., 1999, *A&A*, 348, 737
- Riess A. G., et al., 2016, *ApJ*, 826, 56
- Saha A., Thim F., Tammann G. A., Reindl B., Sandage A., 2006, *ApJS*, 165, 108
- Salo H., et al., 2015, *ApJS*, 219, 4
- Sandage A., Brucato R., 1979, *AJ*, 84, 472
- Schinnerer E., Maciejewski W., Scoville N., Moustakas L. A., 2002, *ApJ*, 575, 826
- Semczuk M., Łokas E. L., de Lorenzo-Cáceres A., Athanassoula E., 2023, arXiv e-prints, p. arXiv:2309.17180
- Sheth K., et al., 2010, *PASP*, 122, 1397
- Shlosman I., Frank J., Begelman M. C., 1989, *Nature*, 338, 45
- Sil'chenko O. K., Afanasiev V. L., 2004, *AJ*, 127, 2641
- Sormani M. C., Treß R. G., Ridley M., Glover S. C. O., Klessen R. S., Binney J., Magorrian J., Smith R., 2018, *MNRAS*, 475, 2383
- Sormani M. C., Sobacchi E., Sanders J. L., 2023, arXiv e-prints, p. arXiv:2309.14093
- Stuber S. K., et al., 2023, *A&A*, 676, A113
- Tamburro D., Rix H.-W., Walter F., Brinks E., de Blok W. J. G., Kennicutt R. C., Mac Low M.-M., 2008, *AJ*, 136, 2872
- Tonry J. L., Dressler A., Blakeslee J. P., Ajhar E. A., Fletcher A. B., Luppino G. A., Metzger M. R., Moore C. B., 2001, *ApJ*, 546, 681
- Valenti E., et al., 2016, *A&A*, 587, L6
- Verheijen M. A. W., Sancisi R., 2001, *A&A*, 370, 765
- Watkins A. E., et al., 2022, *A&A*, 660, A69
- Wegg C., Gerhard O., Portail M., 2015, *MNRAS*, 450, 4050
- Williams T. G., et al., 2021, *AJ*, 161, 185
- Wozniak H., 2015, *A&A*, 575, A7
- Wozniak H., Friedli D., Martinet L., Martin P., Bratschi P., 1995, *A&AS*, 111, 115
- Yuan W., et al., 2020, *ApJ*, 902, 26
- de Vaucouleurs G., 1975, *ApJS*, 29, 193
- de Vaucouleurs G., de Vaucouleurs A., Corwin H. G., Buta R. J., Paturel G., Fouqué P., 1993, *Third Reference Catalog of Bright Galaxies*. New York: Springer-Verlag
- van Driel W., Mulder P., Combes F., 1996, in Buta R., Crocker D. A., Elmegreen B. G., eds, *Astronomical Society of the Pacific Conference Series Vol. 91, IAU Colloq. 157: Barred Galaxies*. p. 253
- van Eymeren J., Jütte E., Jog C. J., Stein Y., Dettmar R.-J., 2011, *A&A*, 530, A29

## APPENDIX A: RESOLUTION EFFECTS

Bars that are too small relative to the resolution of an image can be hard to detect, and may therefore be missed. If bar size has some variance *and* is correlated with a galaxy parameter of interest, such as stellar mass, then a resolution limit can interact with this to produce (or exaggerate) an apparent decrease of bar frequency with change in galaxy parameter: intrinsically smaller bars become probabilistically

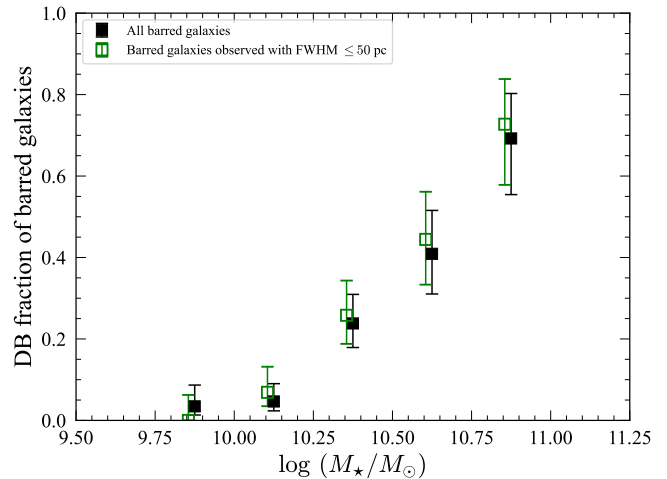


**Figure A1.** As for Figure 2, but showing just the double-bar fraction for all barred galaxies (black squares) and for only those barred galaxies with spatial-resolution FWHM better than 50 pc (open green squares) for the images used for inner-bar identification. The trends are almost identical, suggesting that the results are not strongly affected by varying image resolution.

harder to detect, and so galaxies that tend to have *smaller* bars will appear to have *fewer* bars. Indeed, just such an effect was suggested as the cause for the difference in the observed dependence of bar fraction on galaxy mass between S<sup>4</sup>G and more distant SDSS samples in Erwin (2018). Since there is evidence that inner bars have, like large-scale bars, a dependence on galaxy mass (Figure 9), the possibility of resolution effects is something that should be checked.

A plausible rule of thumb is that a bar should have a semi-major axis at least twice the FWHM of the point-spread function (PSF) of an image (e.g., Aguerri et al. 2009; Erwin 2018; Liang et al. 2023) in order for it to be reliably detected. For a given FWHM in angular size, galaxies at larger distances will have an effective spatial resolution (in pc) worse than galaxies at smaller distances. In addition, this survey relies on a heterogeneous set of observations with a wide range of different angular resolutions, ranging from optical *HST* images (FWHM  $\approx 0.07''$ ) to *Spitzer* IRAC1 images (FWHM  $\approx 1.6''$ ). Given all this, it is worth examining how much varying spatial resolutions could affect the detectability of inner bars and nuclear rings.

The smallest inner bars mentioned in the review of Erwin (2011) have semi-major axes  $\sim 100$  pc (and the smallest bar in *this* paper has  $a_\epsilon = 115$  pc), so we should probably consider that our limit. (Nuclear rings tend to be *larger* than inner bars (e.g., Section 5.) We can therefore consider a galaxy properly resolved if the spatial FWHM is  $< 50$  pc. Figure A1 shows the trend of double-bar fraction versus stellar mass for the entire sample (filled black squares, as for Fig. 2), and then for the “properly resolved” subset containing just those galaxies with spatial FWHM  $< 50$  pc (open green squares). The double-bar fraction is *slightly* higher at all masses  $\log(M_*/M_\odot) > 10.25$ , which suggests the survey as a whole *might* be underestimating the double-bar fraction. But the differences are marginal, and it is plausible to say that two trends are identical within the uncertainties. This provides good evidence that the overall analysis in this paper is *not* strongly affected by resolution issues.

## APPENDIX B: DISCARDED GALAXIES

A total of 25 galaxies were discarded from the initial sample due to being too highly inclined or even edge-on (NGC 3912, NGC 4435, NGC 4606, NGC 4638, NGC 5103, NGC 5493, NGC 5574, NGC 5667, UGC 9215, and PGC 27316); distorted by ongoing interactions or post-merger states, which can make it difficult to properly deproject bar or ring sizes (NGC 274, NGC 275, NGC 2655, NGC 2685, NGC 3227, NGC 3310, NGC 3395, NGC 3414, NGC 4382, NGC 4567, NGC 5195, NGC 5953, NGC 7465, and UGC 5814), or too close to bright stars (IC 630).

Three galaxies were removed for having measured distances outside the 30 Mpc limit: NGC 3021 (Cepheid distance = 31.6 Mpc [Riess et al. 2016](#)); NGC 3504 (surface brightness fluctuation distance = 34.4 Mpc; [Jensen et al. 2021](#)); and NGC 4386 (SBF distance = 30.6 Mpc [Jensen et al. 2021](#)). Six more had group distances (i.e., membership in groups with at least three direct distance measurements) in [Kourkchi & Tully \(2017\)](#) outside 30 Mpc: IC 3102 (31.4 Mpc), NGC 524 (31.2 Mpc), NGC 4269 (31.4 Mpc), NGC 4292 (31.4 Mpc), NGC 4378 (31.4 Mpc), and NGC 5371 (32.0 Mpc). An additional galaxy (NGC 4389) had a group distance small enough (7.3 Mpc) so that its revised stellar mass ( $\log(M_*/M_\odot) = 9.21$ ) put it below the sample cutoff. Finally, NGC 3730 has no distance in  $S^4G$ , and the NED and HyperLEDA redshifts strongly disagree, so I removed it as well.

## APPENDIX C: NOTES ON INDIVIDUAL BARRED GALAXIES

Notes and measurements for the following galaxies can be found in [Erwin & Sparke \(2003\)](#): IC 676, NGC 718, NGC 936, NGC 1022, NGC 2681 (see also [Erwin & Sparke 1999](#)), NGC 2859 (see also [Erwin et al. 2015](#)), NGC 2950, NGC 2962, NGC 3185, NGC 3412, NGC 3729, NGC 3941, NGC 3945 (see also [Erwin & Sparke 1999](#); [Erwin et al. 2003](#); [Erwin et al. 2015](#)), NGC 4143, NGC 4203, NGC 4245 (see also below), NGC 4314, NGC 4386, NGC 4624 (as “NGC 4665”), NGC 4691, NGC 5701, and NGC 7280. [Gutiérrez et al. \(2011\)](#) provides details for NGC 3599 and NGC 3998.

For most other galaxies, the “disc orientation” (PA and inclination) is generally based on the shape of disc isophotes (i.e., from ellipse fits to images) well outside the bar, assuming circularity and an intrinsic disc flattening  $c/a = 0.2$ . The specific image or images used for each galaxy is given in Table 1. Other sources (used when, e.g., outer-disc isophotes were too low in S/N, did not have consistent, unvarying orientations due to strong spiral arms, etc.) are listed below for specific galaxies.

**NGC 514:** Disc orientation from *HST* WFC3-IR F160W image (Proposal ID 16407, PI Grauer).

**NGC 864:** Disc orientation from  $H\alpha$  velocity field ([Epinat et al. 2008](#)). This galaxy has the smallest nuclear ring (deprojected  $a = 99$  pc) in the sample.

**NGC 1068 (M77):** See [Erwin \(2004\)](#) for discussion of evidence for both inner and outer bars, and [Erwin et al. \(2015\)](#) for detailed morphological and kinematic analysis. This galaxy has the largest inner bar in the sample (deprojected  $a_\epsilon = 1.04$  kpc).

**NGC 1637:** Disc orientation from gas velocity fields in [Williams et al. \(2021\)](#).

**NGC 2608:** Disc orientation from *Spitzer* IRAC1 image and 2D decomposition of [Salo et al. \(2015\)](#).

**NGC 2681:** See Section 6.4.

**NGC 2787:** See [Erwin & Sparke \(2003\)](#). The morphology and

stellar kinematics inside the bar were analyzed in detail in [Erwin et al. \(2003\)](#); however, the “inner disc” they identified is more likely to be the projected B/P structure of the bar. The two “dust” rings mentioned in [Comerón et al. \(2010\)](#) are associated with off-plane gas [Erwin et al. \(2003\)](#); [Sil’chenko & Afanasiev \(2004\)](#).

**NGC 2968:** I use the HyperLEDA Hubble-type (SBa) rather than the RC3 I0 classification.

**NGC 3031 (M81):** Although this galaxy was classified as unbarred in [de Vaucouleurs et al. \(1993\)](#), it is actually double-barred ([Gutiérrez et al. 2011](#)). The inner bar was first identified (as a “minibar”) by [Elmegreen et al. \(1995\)](#); the weak outer bar was described by [Gutiérrez et al. \(2011\)](#) and [Erwin & Debattista \(2013\)](#).

**NGC 3368 (M96):** See [Nowak et al. \(2010\)](#) and [Erwin et al. \(2015\)](#).

**NGC 3458:** This galaxy has the smallest inner bar in the sample (deprojected  $a_\epsilon = 115$  pc).

**NGC 3489:** See [Erwin & Sparke \(2003\)](#), [Nowak et al. \(2010\)](#), and [Erwin et al. \(2015\)](#).

**NGC 3626:** Although classified as unbarred by [de Vaucouleurs et al. \(1993\)](#), [Laurikainen et al. \(2005\)](#) and [Gutiérrez et al. \(2011\)](#) found it to be double-barred.

**NGC 3726:** Disc orientation from  $H\ I$  velocity field ([van Eymeren et al. 2011](#)).

**NGC 3982:** The “nuclear ring” noted by [Comerón et al. \(2010\)](#) lies outside the sole bar in this galaxy, and so I consider it an inner ring instead.

**NGC 3992 (M109):** Disc orientation from  $H\ I$  velocity field ([Verheijen & Sancisi 2001](#)).

**NGC 4041:** Small-scale (“nuclear”) single bar in nominally unbarred galaxy (e.g., [Comerón et al. 2014](#)).

**NGC 4051:** Disc orientation from  $H\ I$  velocity field ([Liszt & Dickey 1995](#)).

**NGC 4102:** The “nuclear ring” noted by [Comerón et al. \(2010\)](#) is, in *HST* near-IR images, a complex, possibly off-center structure that is not clearly ringlike, so I do not classify it as a nuclear ring.

**NGC 4151:** Disc orientation from  $H\ I$  velocity field ([Pedlar et al. 1992](#)).

**NGC 4221:** This is the lowest-mass nuclear-ring host galaxy in the sample.

**NGC 4245:** The *HST* WFC3-IR image shows inner bar not visible in optical, ground-based images analyzed by [Erwin & Sparke \(2003\)](#).

**NGC 4250:** Disc orientation from [Salo et al. \(2015\)](#).

**NGC 4303:** Disc orientation from [Schinnerer et al. \(2002\)](#).

**NGC 4319:** Disc orientation from analysis of archival *R*-band images from the Isaac Newton Group.

**NGC 4321 (M100):** Disc orientation from  $H\ I$  velocity field ([Haan et al. 2008](#)).

**NGC 4371:** Disc orientation from [Erwin et al. \(2008\)](#).

**NGC 4608:** See [Erwin et al. \(2021\)](#).

**NGC 4643:** See [Erwin et al. \(2021\)](#), where the stellar nuclear ring suggested by [Erwin \(2004\)](#) is demonstrated to be a nuclear disc with a broken-exponential profile.

**NGC 4699:** See [Erwin et al. \(2015\)](#).

**NGC 4713:** Disc orientation from  $H\alpha$  velocity field ([Epinat et al. 2008](#)).

**NGC 4725:** Disc orientation from a combination of ellipse fits to IRAC1 image and  $H\ I$  velocity field ([Ponomareva et al. 2016](#)).

**NGC 4736 (M94):** Disc orientation from stellar and gas kinematics in [Moellenhoff et al. \(1995\)](#) and [van Driel et al. \(1996\)](#). This galaxy has the largest nuclear ring (deprojected  $a = 1.26$  kpc) in the sample.

**NGC 4750:** See [Gutiérrez et al. \(2011\)](#). This was suggested as possible double-bar by [Erwin \(2004\)](#), with the outer bar being uncertain, primarily due to the low S/N of the 2MASS near-IR images.

The *Spitzer* IRAC1 image shows very clearly that the spiral arms lie in an oval region misaligned with respect to the outer disc. This makes the outer bar somewhat similar to the bar in NGC 5248.

**NGC 4941:** This was suggested as possible but unconfirmed double-bar in [Erwin \(2004\)](#), due to uncertainty about the existence of the outer bar. Evidence for the latter’s reality includes offset gas lanes in detected in CO by [Stuber et al. \(2023\)](#) and also in ionized-gas emission (T. Kolcu, private comm.).

**NGC 5194 (M51a):** Disc orientation from H I velocity field ([Tamburro et al. 2008](#)). [Comerón et al. \(2010\)](#) note the existence of a star-forming “nuclear” ring with  $a = 16.1''$ ; since this is *larger* than the only bar in the galaxy, I do not consider it a true nuclear ring.

**NGC 5248:** I consider the (very) large-scale structure identified by [Jogee et al. \(2002\)](#) to be the bar, rather than the (much smaller) “bar” reported by [Herrera-Endoqui et al. \(2015\)](#). For simplicity, I only list the larger of the two star-forming nuclear rings (the smaller, with  $a \approx 1.5''$ , would be the smallest nuclear ring in terms of size relative to the bar).

**NGC 5377:** [Erwin & Sparke \(2003\)](#) listed *two* nuclear rings in this galaxy. The first, a larger dusty ring, is unambiguous and is the one used here. The second (a “blue” nuclear ring) is perhaps more of a blue nuclear disc, marked by weak inner dust lanes.

**NGC 5457 (M101):** Disc orientation from inner part of HI velocity field ([Bosma et al. 1981](#)).

**NGC 5480:** Disc orientation from CO velocity field ([Levy et al. 2018](#)).

**NGC 5770:** This is the lowest-mass double-barred galaxy in the sample.

**NGC 5806:** Disc orientation from INT-WFC *r* images ([Erwin et al. 2008](#)).

**NGC 5850:** Disc orientation from H I velocity field ([Higdon et al. 1998](#)).

**NGC 5964:** Disc orientation from H I ([Hewitt et al. 1983](#)) and H $\alpha$  ([Hernandez et al. 2005](#)) velocity fields.

**NGC 6412:** Disc orientation from H $\alpha$  velocity field ([Epinat et al. 2008](#)).

**NGC 7741:** Disc orientation from IRAC1 and H $\alpha$  velocity field ([Fathi et al. 2009](#)).

**NGC 7743:** See [Erwin & Sparke \(2003\)](#). An updated discussion of the orientation of this galaxy can be found in [Davies et al. \(2014\)](#).

**PGC 12633:** Disc orientation from IRAC1 and SGA images.

This paper has been typeset from a  $\text{\TeX}/\text{\LaTeX}$  file prepared by the author.